SIMULATION OF AUTOMOTIVE EMISSION CONTROL SYSTEMS

Mehrdad Ahmadinejad, Maya R. Desai, Timothy C. Watling* and Andrew P.E. York

Johnson Matthey Technology Centre, Blount's Court, Sonning Common, Reading, RG4 9NH, UK

Abstract

As emissions requirements become evermore stringent, designing a system to meet the legislation subject to packaging and cost constraints becomes progressively more difficult. This is further exacerbated by increasing system complexity, where more than one technology may be required to control all the legislated pollutants and/or an active

*Corresponding author. Tel.: +44(0)118 924 2139; Fax: +44(0)118 924 2106.
E-mail: watlit@matthey.com

Advances in Chemical Engineering, vol. 33
ISSN 0065-2377
DOI 10.1016/S0065-2377(07)33002-0

regeneration strategy is involved. By using computer simulation to aid design, this process can be considerably shortened, saving time and money. As an added bonus, the exercise of model development and application can lead to a greater understanding of the chemistry and physics of the system.

This chapter gives an overview of some of the work done at Johnson Matthey on simulating emissions control devices. It covers both model development and the application of modelling to aid the design of exhaust aftertreatment systems. Simulation of the majority of emissions control technologies is covered, viz. 3-way catalysts for gasoline exhaust; and oxidation catalysts, urea/ammonia selective catalytic reduction, NO_X traps and particulate filters for diesel exhaust. Examples of the application of modelling to consider parameters such as substrate (monolith) type, catalyst size and aspect ratio, engine calibration and precious metal loading and distribution are given.

I. Introduction

As emissions requirements become evermore stringent (Heck and Farrauto, 2001), designing a system to meet the legislation subject to packaging and cost constraints becomes progressively more difficult. This is further exacerbated by increasing system complexity, particularly for diesel exhaust, where separate technologies may be used for NO_X and particulate control and active regeneration strategies involved. Even with the well-established 3-way catalysts (TWCs) used for gasoline exhaust, there is likely to be more than one catalyst, each with a different precious metal loading and combination/selection of platinum, palladium and rhodium and/or support (washcoat) to obtain optimum reactivity. Thus, designing an aftertreatment system by a "trial and error" approach becomes more protracted and expensive; it is not just testing that is time consuming, but also preparation of catalysts, aging and mounting. By using computer simulation to aid design, this process can be considerably shortened. As an added bonus, the exercise of model development and application can lead to a greater understanding of the chemistry and physics of the system.

In recent years there has been an increase in interest in simulation of automotive aftertreatment systems both among academics (Marin and Hoebink, 1997), catalyst manufacturers (Ahmadinejad *et al.*, 2006; York *et al.*, 2005), vehicle/engine producers (Baba *et al.*, 2000; Laing *et al.*, 1999; Oh and Cavendish, 1982) and consulting companies (Wanker *et al.*, 2002). A lot of this work is published in the open literature, however, there is a limit to what industry will publish, in order to maintain a competitive advantage. In particular, kinetic equations and especially kinetic parameters are generally

regarded as proprietary information and hence are rarely seen in published work.

This chapter discusses both the development of models and their application. One way of organising this chapter would be to discuss model development first and then go on to consider the applications. However, as the entire reason for developing these models is to have a practical tool for system design, it was decided to start with the application of the models. The next section discusses the physical model for a monolith reactor, which is common to all technologies (except diesel particulate filters) discussed later. Our approach to model development will then be covered in detail, using TWCs as an example. The final section will outline work done on the various technologies used for diesel exhaust aftertreatment.

II. Applications of Modelling/Rational Design of Emissions Control System

As we develop aftertreatment system models to be used as a practical tool for system design rather than as an exercise in itself, this chapter will start by discussing the applications of modelling. Since catalyst kinetics must be empirically determined (until molecular modelling advances considerably), modelling cannot help in catalyst design, i.e. to design the chemistry. However, it can be used to aid designing an aftertreatment system, i.e. to use the chemistry to its best advantage. In an age where computer simulation is used in someway to design almost every component of a vehicle, it seems logical that computer simulation should be used to assist in the design of the aftertreatment system. Given the complexity of the chemistry involved, it seems unlikely that computers will replace testing in the near term, and indeed experimental testing is generally required by legislation. However, computer simulation can be used to examine a wide range of alternatives quickly and cheaply, enabling testing to be confined to only the most promising systems, thereby leading to a faster design process. Figure 1 illustrates some of the many variables in an emissions system that can be investigated with computer simulation.

Computer simulation can be used to consider not only the effect of the emissions system itself, but also the effect of engine design. For example, the effect of recalibrating the engine to produce hotter exhaust gas or a different gas composition can be considered without actually doing this on the engine until the result is known to be worthwhile. The rest of this section will consider these two aspects separately. All the examples shown in this section are for TWCs.

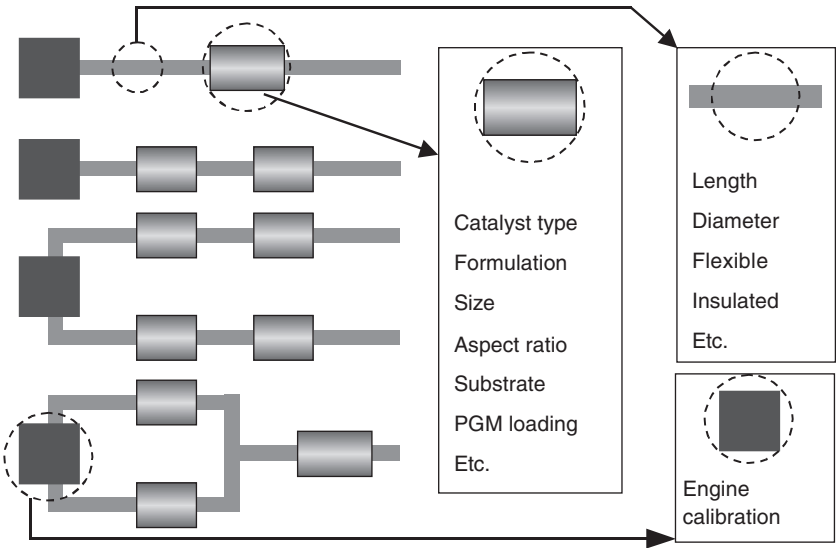

FIG. 1. Schematic illustrating possible configurations of engine (dark square), catalyst(s) (grey rectangles) and connecting pipes together with potential system variables.

A. CATALYST SYSTEM DESIGN

Before discussing system parameters, which modelling can help define, it is worth briefly outlining the construction of the catalytic converter for those not familiar with them. The converter consists of a substrate (the physical support), which is generally either a ceramic monolithic honeycomb with square channels or a metallic monolith formed by winding flat and corrugated metal foils together, onto which the active component, known as the washcoat, is coated. The washcoat consists of the chemical support onto which the active metal is dispersed (Twigg, 2007).

Computer simulation can be used to consider a wide range of system parameters, such as

- different formulations, precious metal loading and aging (if suitable kinetics available);
- number of catalysts;
- proximity to engine;
- exhaust pipe (single or dual skin, flex coupler, length, diameter);
- catalyst size and aspect ratio and
- substrate choice (cell density, wall thickness; ceramic or metallic).

It is worth expanding on some of these points. Modelling can be used to look at the (support) formulation, precious metal loading and catalyst aging,

provided suitable catalyst kinetics are available. It is an unfortunate fact that chemical kinetics must be empirically determined for each catalyst formulation and aging, and that this can be a time consuming process even for just one catalyst/aging. However, this process can be simplified by perhaps doing a detailed kinetics study (as described in Section IV) on a sample of a given formulation with a representative aging and precious metal loading and then doing a smaller kinetics study on other samples with different aging and/or metal loadings, and fitting the data using a subset of the kinetics parameters. Typically, it is assumed that the metal loading and aging affects only the number of sites, but not the activity of individual sites. In the absence of better information, it is often assumed that the catalyst activity is linearly proportional to precious metal loading. While this approximation often works well, it is not always correct (Evans *et al.*, 1999). Finally, it is worth remembering that sometimes catalyst activity is not the limiting factor in controlling emissions. For example, in a vehicle where the exhaust temperature ramps-up rapidly after key-on, catalyst light off may be limited not by catalyst activity, but by the rate at which the catalyst warms up. In this case, increasing the rate of the kinetics (equivalent to increasing metal loading or using a more advanced washcoat (support)), will have no effect on the predicted emissions.

Heat losses from the exhaust gas, as it travels down the exhaust pipe from the engine to the catalyst, result in slower catalyst warm-up and reduced conversion. These heat losses can be reduced by moving the catalyst closer to the engine or by using a dual skin (insulated) exhaust pipe rather than a standard single skin pipe. The diameter of the exhaust pipe will also have an effect. By using a model for heat losses from the exhaust pipe, such as that published by Ansell *et al.* (1996), such effects can be quantified.

Clearly substrate type and catalyst size can have a significant effect on post-catalyst emissions. Figure 2 shows an example of a study looking at this on a TWC. The simulations were run for the first 200s of the FTP (Federal Test Procedure; a standard US drive cycle) test as catalyst light off was of prime interest. Only predicted THC (total hydrocarbon) emissions are discussed here. The base case (line 1) was a 5.66×6 in (144×152 mm), 400/6 (i.e. 400 cells per square inch with 6/1,000 in wall thickness) catalyst. This was replaced by a so-called "cascade" system, consisting of a 4×4 in (102×102 mm) catalyst followed by a 5.66×4 in (144×102 mm) catalyst in the same can. This system has the same total catalyst volume as the original system. In the simulations, it was assumed that the cone between the two substrates was ideally designed so that the gas flow across the front face of the rear catalyst was even. Line 2 is the predicted THC emissions for just the front catalyst. The smaller front face area of the 4×4 in catalyst compared to the original 5.66×6 in catalyst, means that the heat of the exhaust is taken up by a smaller area, leading to earlier light off. However, the smaller volume of the 4×4 in part results in larger breakthrough after light off, so the benefit of earlier light off is soon lost. With the full cascade system (line 3), the extra volume of the second catalyst results in reduced

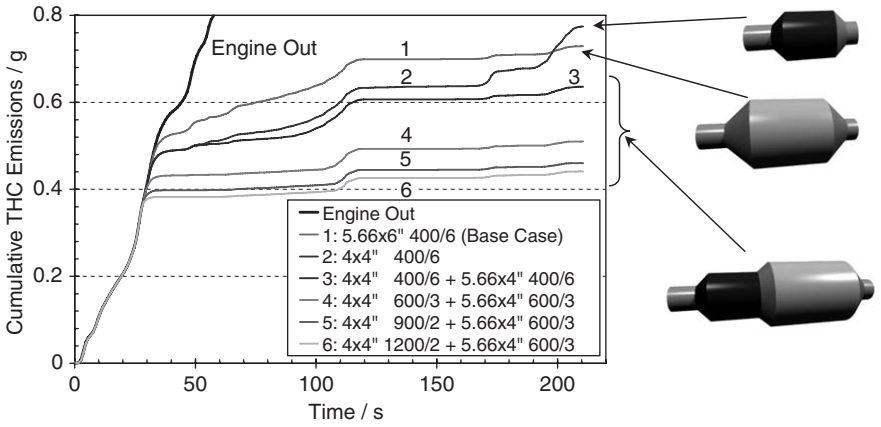

FIG. 2. Predicted THC emissions during the first 210s of the FTP showing the effect of substrate type and of having one or two catalysts. The single catalyst (5.66×4 in/144×152 mm) and two catalyst ($4 \times 4 + 5.66 \times 4$ in/102×102 mm + 144×102 mm) systems have the same total volume. Substrates are denoted as cells per square inch/wall thickness in thousandths of an inch.

breakthrough after light off, maintaining the advantage of the reduced front face area.

The remaining simulations in Fig. 2 look at changing the substrate type. Line 4 shows the predicted effect of changing both 400/6 substrates for 600/3, while lines 5 and 6 show the predicted effect of changing the front substrate to a 900/2 and a 1,200/2, respectively. Substrate choice has two main effects. Lower thermal mass (associated with thinner walls, use of less dense ceramic or even a lower catalyst washcoat loading) leads to faster warm-up and hence earlier light off. Increasing cell density increases geometric surface area and reduces hydraulic diameter, resulting in improved heat and mass transfer between the exhaust gas and the substrate, leading to faster warm-up and hence reduced breakthrough after light off. Examination of Fig. 2 reveals that increasing cell density and reducing wall thickness, does indeed result in earlier light off and reduced breakthrough after light off. Note that going from a 900/2 front catalyst to a 1,200/2 (lines 5 and 6) is predicted to have a relatively small effect. This is because the higher thermal mass of the 1,200/2 (more walls of the same thickness) offsets the advantage of greater heat transfer.

It is worth noting that all the simulation results shown in Fig. 2 were run with the same engine out data, i.e. it was assumed that changing the substrate(s) did not affect the emissions from the engine. In reality, increasing the substrate cell density is likely to increase the backpressure, which in turn may affect the engine out emissions; this effect is not included in this model. On the plus side, running each simulation with the same engine out data avoids any problems

with test reproducibility, which is found with experimental chassis dynamometer data, especially if a human driver is used.

Another example of the use of modelling to consider substrate choice can be found in Lafyatis *et al.* (2000).

B. Modification of Engine Calibration

It is important to remember that the aftertreatment system does not work in isolation, but is part of a system with the engine. Clearly, the composition of the exhaust gases, their temperature and flow rate influence the catalyst performance. With a gasoline engine, the combustion must take place close to stoichiometry, if a TWC is to be able to control CO, NO_X and THC emissions. With diesel engines, some complicated engine management may be required for regeneration, e.g. running the engine rich to regenerate a NO_X trap, or making the exhaust hotter to regenerate a soot filter. Exhaust temperature is, of course, another key factor affecting rate of reaction over the catalyst. By using simulation, the effect of a change in the engine calibration (i.e. the way the engine runs) can be assessed simply by modifying existing engine out data to see if such a change in the calibration is worthwhile. Only if the calibration change is likely to be useful, do the calibration engineers need to make the necessary changes, thus potentially saving much time and effort. This section looks at two examples for a gasoline engine, considering the influence of the initial temperature ramp and of reducing engine out HC levels before light off.

The predicted effect of initial temperature ramp on THC emissions during the first 210s of the FTP test is shown in Fig. 3. These simulations were run by modifying the original engine out data, which had an initial ramp of about 6 K/s, to one with a faster, linear ramp (Fig. 4). As expected, increasing the initial ramp rate results in faster catalyst warm-up and hence earlier light off. However, the extent of improvement in light off with increasing temperature ramp decreases as the ramp rate is increased. Thus, while going from 6 to 10 K/s has a large effect, doubling the ramp rate to 20 K/s has a smaller, but still significant effect; little is to be gained from increasing the ramp rate beyond 35 K/s. With these results, the cost/difficulty of getting the increased temperature ramp from the engine can be weighed up against the potential savings from the use of a smaller and/or lower precious metal loaded catalyst. These predictions also make it clear that there is a limit on the maximum ramp rate that is worth considering with this system. It may be that if a higher cell density substrate were used, the heat transfer to the catalyst would be improved, and more benefit would be seen for the more rapid temperature ramps.

It is interesting to observe that, increasing the initial temperature ramp not only results in earlier light off, but also results in reduced breakthrough after light off. Figure 3 clearly shows that the predicted breakthrough at

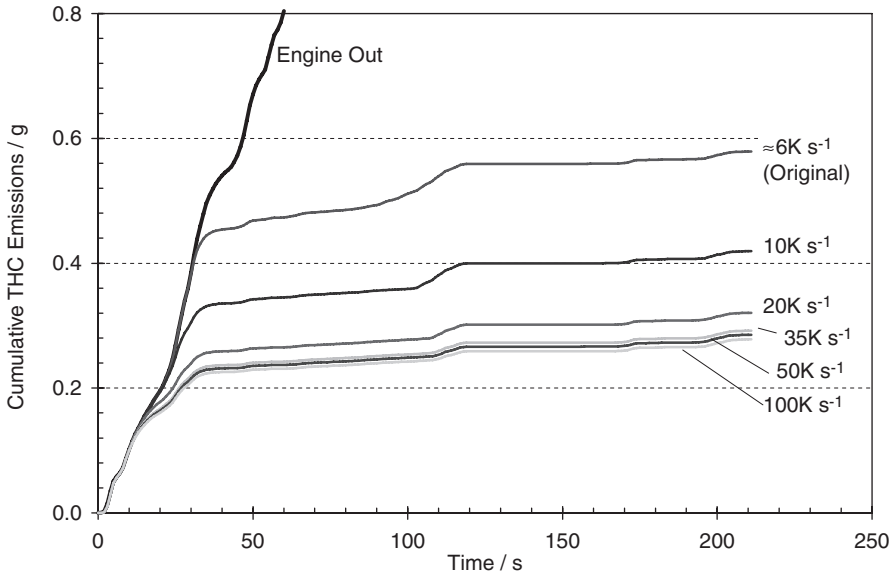

FIG. 3. Predicted effect of initial temperature ramp on HC emissions over the first 210s of the FTP test. The inlet temperatures used are shown in Fig. 4.

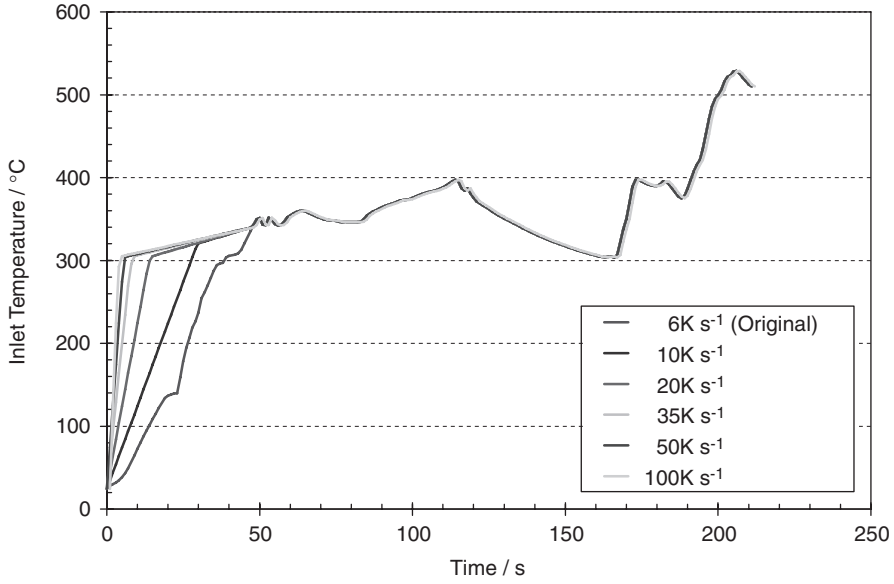

FIG. 4. Inlet temperatures fed to the model to predict the effect of initial temperature ramp. The measured data have an initial temperature ramp of $\sim 6\,\mathrm{K/s}$.

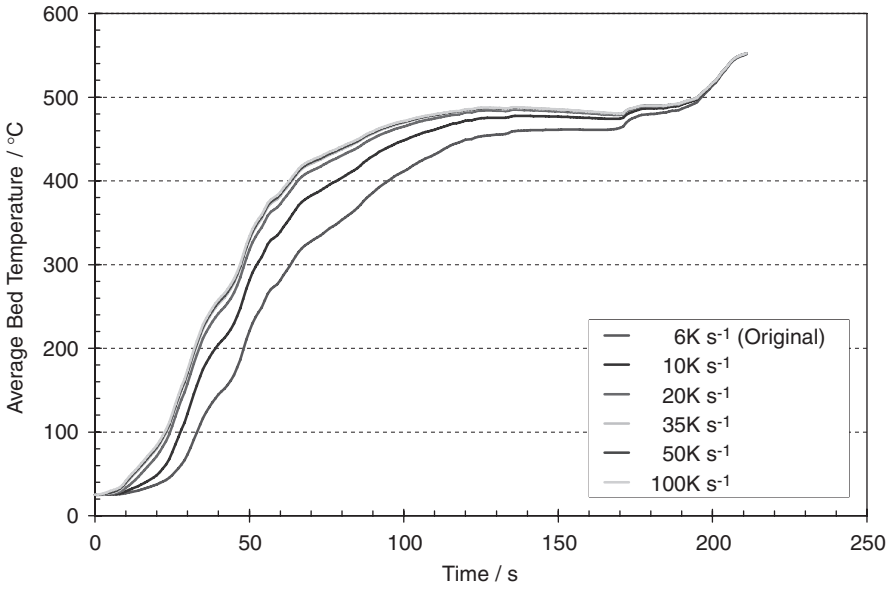

FIG. 5. Predicted average catalyst temperature as a function of initial temperature ramp rate.

about 100s decreases with increasing ramp rate, even though the inlet temperature for all simulations is the same after 50s (Fig. 4). Examination of the predicted average catalyst temperature (Fig. 5) reveals that the effect of the brief initial temperature ramp still has an influence on catalyst temperature until 195s into the test. This is presumably due to extra heat generated by CO and HC combustion, on account of earlier light off. Since the catalyst is hotter, the size of the breakthrough at 100s is reduced. This example illustrates how a better understanding of the system can be gained by examining parameters predicted by the model.

The second example considers changing the engine calibration to reduce engine out HC. Since a large portion of post-catalyst HC emissions is released before the catalyst lights off, reducing HC output at the beginning of the test can be very beneficial. Figure 6 shows the predicted effect of reducing engine out HC to one-half and one-third of the measured values. As expected, reducing the engine out HC resulted in reduced catalyst out HC. However, the catalyst out emissions are actually slightly lower than expected from the reduction in engine out HC. This is because HC inhibits CO and HC oxidation, so reducing the HC going into the catalyst results in a faster rate of reaction, and hence more heat generation leading to a further increase in the reaction rate.

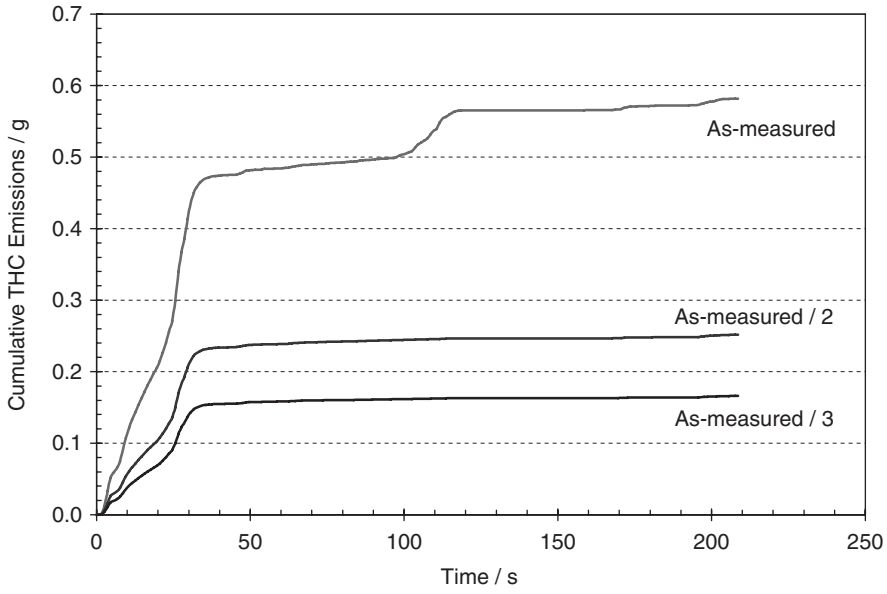

FIG. 6. Predicted effect of reducing engine out HC to one-half and one-third of the as-measured levels on THC emissions during the first 210s of the FTP.

III. Monolith Reactor Model

In this section, the physical model used to describe the flow-through monolith reactor is outlined. Such a reactor is common to all the emissions control strategies discussed in this chapter, apart from soot filters.

A brief review of the development history of monolith reactor models for TWC applications can be found in Koltsakis and Stamatelos (1997). Various workers have looked at 1-, 2- and 3-dimensional models considering both the whole monolith and just a single channel. A multidimensional model for the whole monolith is required for investigating the effects of a flow maldistribution across the front face of the monolith, but is probably unnecessary when the flow is uniform. Other workers have studied multidimensional single channel models, where the gas flow within the channel is modelled in detail. In general, for a model to be useful in practice, some compromise has to be made between having a reasonable runtime versus detail/complexity, both in terms of the chemical kinetics and the description of the flow field within the channels of and across the monolith.

Most of our work has focused on 1-dimensional models, as these give a reasonable runtime, at the expense of ignoring radial gradients; for a

well-designed system, where the flow across the front face of the catalyst is uniform, this is a good approximation.

Our model has been previously published (Ansell *et al.*, 1996) and is similar to that of other workers in the field (e.g. Baba *et al.*, 2000; Marin and Hoebink, 1997; Oh and Cavendish, 1982); such models are well established, hence our main focus is on the chemistry/kinetics of our aftertreatment catalysts.

The model is a 1-dimensional lumped parameter model with the following assumptions:

- Uniform flow distribution at the entrance to monolith.
- Negligible radial temperature gradient across the monolith.
- Axial transport of mass and energy in the gas phase by convection only.
- Axial transport of energy in the solid phase by conduction.
- Transfer of mass and energy between the gas and solid phases described by mass and heat transfer terms with coefficients calculated from a correlation based on Ullah *et al.* (1992).
- No radiative transport of energy to or from the monolith faces.
- No diffusion resistance in the washcoat.
- Reactant gases are dilute so that changes in the amount of substance (and hence gas volume) with reaction can be ignored, i.e. this is a trace system.
- Negligible pressure drop along the channels.
- Ideal gas behaviour.

The equations describing the 1-dimensional model are

$$0 = \rho_g C_{pg} v \frac{\partial T_g}{\partial z} + h\, S_v (T_g - T_s) + h_o \frac{2}{r}(T_g - T_{surr}) \quad \text{Gas energy balance} \tag{1}$$

$$0 = \frac{\partial v C_{gi}}{\partial z} + k_{m,i} S_v (C_{gi} - C_{si}) \quad \text{Gas mass balance} \tag{2}$$

$$(1-\varepsilon)\rho_s C_{ps} \frac{\partial T_s}{\partial t} = (1-\varepsilon)\lambda \frac{\partial^2 T_s}{\partial z^2} - L \sum_i H_i R_i + h\, S_v (T_g - T_s) \quad \text{Solid energy balance} \tag{3}$$

$$(1-\varepsilon)\varepsilon_{wc} \frac{\partial C_{si}}{\partial t} = k_{m,i} S_v (C_{gi} - C_{si}) + R_i L \quad \text{Solid mass balance} \tag{4}$$

where

C_{gi}	concentration of species i in the gas phase	mol/m^3
C_{si}	concentration of species i in the solid phase	mol/m^3
C_{pg}	specific heat capacity of gas phase at constant pressure	J/kg/K

C_{ps}	specific heat capacity of solid phase at constant pressure	J/kg/K
H_i	heat of formation of species i (negative for exothermic reaction)	J/mol
h	heat transfer coefficient for transport between solid and gas phases	$W/m^2/K$
h_o	heat transfer coefficient for heat loss to the surroundings	$W/m^2/K$
$k_{m,i}$	mass transfer coefficient for species i	m/s
L	mass of catalyst per unit volume of monolith	kg/m^3
r	radius of monolith	m
R_i	rate of formation of species i per unit mass of catalyst	mol/kg/s
S_V	geometric surface area (surface area of channels/volume of monolith)	m^{-1}
t	time	s
T_g	temperature of the gas phase	K
T_s	temperature of the solid (monolith)	K
T_{Surr}	temperature of surroundings	K
V	mean velocity of gas in channel	m/s
Z	axial distance	m
ε	open frontal area of monolith	–
ε_{WC}	washcoat porosity × volume of washcoat/solid volume of monolith	–
λ	thermal conductivity of coated monolith	W/m/K
ρ_g	density of gas	kg/m^3
ρ_s	solid density of monolith	kg/m^3

These equations are the same as for the model presented by Ansell *et al.* (1996), with the addition of a term for heat loss to the surroundings in the gas energy balance and with the correction of minor typographical errors.

While Eq. (1) includes a term for heat losses to the surroundings, it is important that this term is relatively minor as significant heat losses will result in a significant radial temperature gradient, which in turn invalidates the use of a 1-dimensional model. In practice, the small surface area to volume ratio of the monolith, and the fact they have some insulation, means that the heat losses are indeed small.

The gas energy and mass balance equations, unlike the corresponding solid balances, do not have a term for accumulation. This is because the high convective flow of gas through the channels of the monolith makes accumulation of heat or reactants in the gas phase negligible. In practice, the accumulation term in the solid mass balance could also be removed as, in general, it also tends to be small. However, it is included in our models as it enables the equations to be solved numerically more easily.

It is worth noting, that while this model would generally be described as a 1-dimensional model, because it contains a single spatial coordinate (z), mass and heat transport between the gas and solid phases within the channel and

perpendicular to the axial direction are included in the model using a lumped parameter approach. Thus, this model might better be described as a single channel model.

IV. Model Development, Illustrated by 3-Way Catalysis

In this section the stages and some of the considerations in developing a model are discussed. All the examples are taken from 3-way catalysis, but the same general principles apply for any other emissions control technologies.

TWCs are used on gasoline vehicles and are so called because they remove three pollutants from the exhaust gas, viz. CO, hydrocarbons and NO_X. They work by reacting the oxidising components of the exhaust (NO_X and O_2) with the reducing components (CO and hydrocarbons). Provided the fuel/air mixture combusted in the engine is stoichiometric, the pollutants effectively "cancel each other out". More information on the chemistry and history of the development of these catalysts can be found in Chorkendorff and Niemantsverdriet (2003), Gandhi *et al.* (2003), Koltsakis and Stamatelos (1997) and Twigg (2007).

A. Approach/Methodology

Ultimately a model is a simplification of real-world behaviour. To be useful, it must produce predictions of sufficient accuracy in a reasonable time span; if it is quicker to do the experiments than to develop and run the model, then the model is worthless (except as an academic exercise). In choosing an approach for modelling a system, a compromise must be made between complexity and simplicity. A very complex model, which includes a detailed description of the many physico-chemical processes involved, may give an accurate prediction over a wide range of conditions. However, there will be many parameters to set from experimental data, and so development and validation will be time consuming. An over complex model may also have a protracted run-time. However, a very simple model may be quick to develop and run, but if the predictions are far from reality, this model is also useless.

The simplest approach used for autocatalyst modelling is the so-called look up table (Laing *et al.*, 1999). Essentially, the model is populated with a database of conversions for various species as a function of temperature and space velocity, from which conversions can be predicted by interpolation. This, coupled with a simple thermal model for catalyst temperature and some way of allowing for mass transport control, constitutes the simplest type of model. Once this sort of model has been written, adapting to another formulation is a relatively quick process of measuring new conversion curves and adding these to the model.

Since the models are so simple, a whole test cycle can be simulated in a very short time. The disadvantage of such a model is that it is not based on the underlying chemical processes and so the range of applicability is likely to be limited.

At the other end of the spectrum lies micro-kinetic modelling (Koči *et al.*, 2004; Marin and Hoebink, 1997). Here not just the individual reactions, but also all the intermediate mechanistic steps are modelled. This leads to a vast number of parameters that must be fixed either from experiment or by theoretical calculations. As a very detailed description of the chemistry is included, an accurate prediction over the widest range of conditions can be expected, provided the correct mechanistic steps and parameters have been chosen. The problem with this approach lies in the time taken to run and, in particular, to develop such a model; an entire PhD thesis can be spent just determining the kinetics of a few of the many reactions required. In the commercial world, the catalyst formulation may well have changed over this period. While such models are interesting and important for understanding in detail the complex chemistry occurring on the catalyst surface, the protracted development time compared to the time taken to bring a commercial catalyst to market makes them unsuitable for use in industry.

At Johnson Matthey, we have adopted an approach somewhere in between these two extremes. The model should reflect the underlying physico-chemical processes involved, to be as predictive as possible over as wide a range of conditions as possible, but yet not be too time consuming to develop and run. A single global rate equation is used for each reaction, thus the chemistry of the catalyst can be included, without creating excessive parameters to define. Typically, Langmuir-Hinshelwood kinetics (Chorkendorff and Niemantsverdriet, 2003) are used, as is normal for reactions occurring on the surface of a heterogeneous catalyst. These equations also behave well numerically; unlike a power law equation, there is no danger of division by zero when concentrations go to zero. A typical rate equation would be

$$r_j = \frac{A_j \exp\left(\frac{-E_j}{RT_s}\right)[A]^m[B]^n}{(1+K_a[A])^p(1+K_b[B]+K_c[C])^q} \tag{5}$$

where r_j is the rate of reaction, A_j the pre-exponential factor, [A], [B], [C] concentrations of A, B and C, E_j the activation energy, R the molar gas constant, K_a, K_b and K_c are Langmuir-Hinshelwood constants, and p, q, m and n are positive constants, ideally integers. Note that the rate of reaction depends not only on the concentrations of the reactants, but also on the concentrations of other species that may inhibit the reaction. Other workers using this approach include Baba *et al.* (2000) and Oh and Cavendish (1982).

The methodology devised for model development is shown in Fig. 7. Data for developing the model come from SCAT (simulated catalyst activity test,

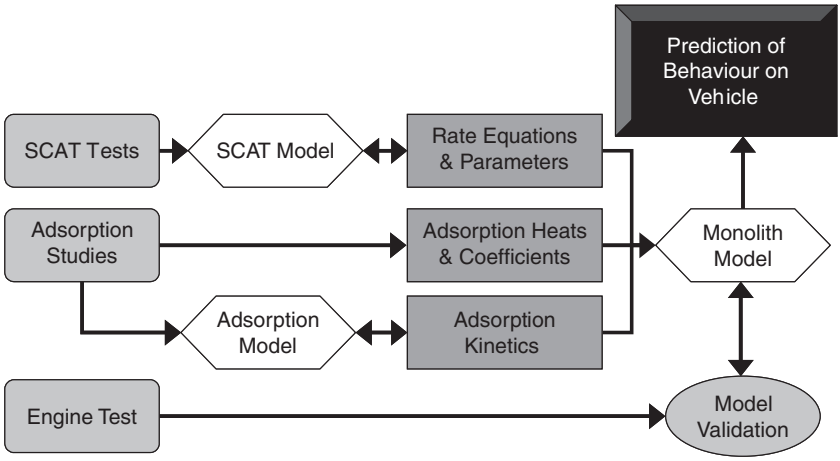

FIG. 7. Model development methodology.

i.e. microreactor) tests, adsorption studies and from real-world engine or vehicle tests.

SCAT data (laboratory microreactor data) are used for development of kinetics. Catalyst testing with synthetic gas mixtures allows for greater and more reproducible feed than is possible when using the exhaust of a real engine. This control is essential for separating out the effects of the many reactions occurring over the catalyst in the complete system. To minimise the influence of heat and mass transfer on the measured conversions, and hence to measure as close to the intrinsic kinetics as possible, these tests are normally done using a packed bed obtained by grinding and sieving an aged monolith catalyst to give tiny catalyst pellets of well-defined size. The SCAT data is then modelled using a model of the SCAT reactor. This is similar to the model described in Section III, except that different correlations, appropriate for a packed bed, are used for the heat and mass transfer coefficients. By trying various forms of kinetic equations and optimising the parameters in these, a series of rate equations with parameters is obtained. This process is discussed in more detail in Section IV.C.

For some models adsorption or storage is important. For example, oxygen storage is important in a 3-way catalysis, a catalyst may contain a hydrocarbon storage component for improved low-temperature performance, and ammonia storage is important for ammonia SCR (selective catalytic reduction). Clearly, this sort of behaviour needs to be included in the final model. The nature of the measurements depends on the exact system being studied and will be discussed in more detail later. Suffice to say, from measurements at steady state, the heats of adsorption and coefficients of

adsorption, i.e. thermodynamics of adsorption, can be determined, and by fitting the rate at which steady state is achieved with a model, a description of the kinetics of adsorption/desorption can be found.

Once the above-discussed components of the model have been determined, they are added to the final model of a monolith (or even filter) reactor. The monolith reactor model has already been described in Section III. The next stage is to validate the model by comparing the predictions of the model based on laboratory data, with the real-world data measured on an engine bench or chassis dynamometer. At this stage the reason(s) for any discrepancies between the prediction and experiment need to be determined and, if required, further work on the kinetics done to improve the prediction. This process can take a number of iterations. Model validation is described in more detail in Section IV.D. Once all this has been done the model can be used predictively with confidence.

B. Reactions Involved

Vehicle exhaust is a complex mixture of many components. This leads to there being potentially a huge number of chemical reactions occurring on the surface of the catalyst, all competing for common reactants and active sites. When developing a model, the trick is to select the salient reactions so that the main features of the catalytic performance can be predicted, without making the model unduly complicated. In this section, the typical reactions included in a TWC model are outlined.

Firstly, reactions of hydrocarbons will be discussed. Vehicle exhaust contains a complex mixture of hydrocarbons (Kubo *et al.*, 1993). These will have different reactivity and their different molecular masses lead to different propensities for mass transport, the larger molecules diffusing more slowly to the catalyst coating. While the full (vast) range of hydrocarbons in the exhaust could not practically be included in a model, it is desirable to include a small number of representative hydrocarbons to emulate the range of activity and transport properties of the full mixture.

Potential reactions of hydrocarbons are total oxidation, partial oxidation and steam reforming. These are shown below, using propene as an example, but similar equations would apply for other hydrocarbons.

$$C_3H_6 + 4\tfrac{1}{2}O_2 \rightarrow 3CO_2 + 3H_2O \quad \text{Total oxidation}$$
$$C_3H_6 + 3O_2 \rightarrow 3CO + 3H_2O \quad \text{Partial oxidation}$$
$$C_3H_6 + 3H_2O \rightarrow 3CO + 6H_2 \quad \text{Steam reforming}$$

Under lean conditions, total oxidation would be expected to be the most important reaction. However, under rich conditions partial oxidation and

steam reforming (especially at higher temperatures) are important contributors to hydrocarbon conversion. Note that partial oxidation and steam reforming produce CO and H_2, which can go on to react with, for example, NO_X.

Oxidation is an important route for CO removal. CO can also react with water in the so-called water gas shift reaction to form H_2. This reaction is important for conversion under rich conditions, at higher temperatures. CO is also an important reductant for NO_X.

$$\begin{aligned} &CO + \tfrac{1}{2}O_2 \rightarrow CO_2 && \text{CO oxidation} \\ &CO + H_2O \rightleftharpoons CO_2 + H_2 && \text{Water gas shift reaction} \end{aligned}$$

Nitrogen oxides (NO_X) are removed by reaction with the reducing species present, viz. CO, H_2 and hydrocarbons. The activity for NO_X reduction increases in the order hydrocarbon $<$ CO $<$ H_2.

$$\begin{aligned} &NO + CO \rightarrow \tfrac{1}{2}N_2 + CO_2 && NO_X \text{ reduction by CO} \\ &NO + 2\tfrac{1}{2}H_2 \rightarrow NH_3 + H_2O && NO_X \text{ reduction by } H_2 \\ &9NO + C_3H_6 \rightarrow 4\tfrac{1}{2}N_2 + 3CO_2 + 3H_2O && NO_X \text{ reduction by hydrocarbon} \end{aligned}$$

Finally, H_2 can be oxidised to water.

$$H_2 + \tfrac{1}{2}O_2 \rightarrow H_2O \quad H_2 \text{ oxidation}$$

Figure 8 is a schematic diagram showing the main reactions together with the temperature required for reaction and the stoichiometry (lean/rich) for which they are important.

C. Developing Kinetics from Microreactor Data

Having good kinetics is the key to having a good model. As already mentioned in Section III, the physical model for a monolithic reactor is well established (validated) and comparable to that used by other workers in the field. It is thus the kinetics used that determine how good the prediction of the model will be. For this reason, the focus of our modelling effort is to develop the best possible kinetics.

Chemical kinetics must be determined empirically. In the future, with developments in molecular modelling, it may one day be possible to predict the kinetic behaviour of a new catalyst formulation without actually making it. However, that day is a long way off, especially given the complex formulation

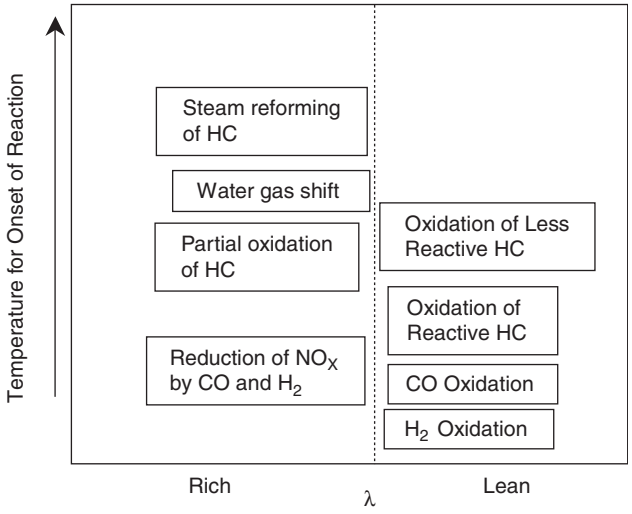

FIG. 8. Schematic showing the importance of the main reactions for a TWC as a function of stoichiometry and temperature required for reaction.

of a modern TWC. Until then, a new set of kinetics will have to be developed for each formulation of interest, and developing good kinetics will remain a time consuming process. It is worth noting that a given set of kinetics is valid not just for a specific formulation but also for a specific aging; as a catalyst ages, so the kinetics will change.

Probably the most cited paper on autocatalyst kinetics is the pioneering work of Voltz *et al.* (1973). This reports kinetics for carbon monoxide and propene oxidation over Pt/Al_2O_3 under oxidising conditions. Many subsequent workers (e.g. Baba *et al.*, 2000; Oh and Cavendish, 1982), without the time and/or equipment to develop new kinetics for their own catalysts, have adapted these kinetics to match either microreactor or engine data. However, given that kinetics are catalyst specific and that generally the formulation is more complicated than just Pt/Al_2O_3, this approach is somewhat unsatisfactory. Moreover, Schweich (1995) has pointed out some shortcomings of these kinetics, for example the heat of adsorption of NO is endothermic, which seems unlikely.

There are a number of kinetics studies of TWCs in the literature. However, those that actually give kinetic expressions and parameters tend to be of model, rather than fully formulated, catalysts. Catalyst manufacturers tend to regard catalyst kinetics as proprietary information and so do not publish them in the open literature.

Having established the importance of generating kinetics, a methodology, which has been found to work well, will be discussed. As already mentioned in

Section IV.A, packed bed microreactor light-off data are the main source of information for generating kinetics. All these measurements are done with CO_2 and water in the feed, as this is always present in vehicle exhaust. These components have an inhibiting effect, but once the concentration is above a certain amount, a further increase in concentration has no significant further inhibiting effect, so the concentration dependence of CO_2 and water can be neglected, provided they are present at a representative level in all experiments.

Figure 9 shows a typical series of CO light-off curves measured under lean conditions. The first curve (squares) is for a simple feed of CO and O_2 (plus CO_2 and water, with N_2 as the balance). In reality, a series of these curves would be measured with different CO and O_2 concentrations, to determine the concentration and temperature dependence of CO oxidation. By modelling this data, a rate expression for CO oxidation for this catalyst can be determined.

The other curves in Fig. 9 show the effect of adding extra components into the feed, which are not actually involved in CO oxidation. These extra components also adsorb on active sites on the catalyst surface and hence inhibit CO oxidation. Thus, adding NO (triangles) or C_3H_6 (circles) to the feed inhibits CO oxidation, shifting the light-off curve to higher temperature. When both NO and C_3H_6 are present (diamonds), the reaction is even further inhibited and the light-off curve is shifted to even higher temperature. Having fixed the rate equation for CO oxidation alone from the $CO + O_2$ only data, further terms can be added to the rate equation to allow for the inhibiting effect of other

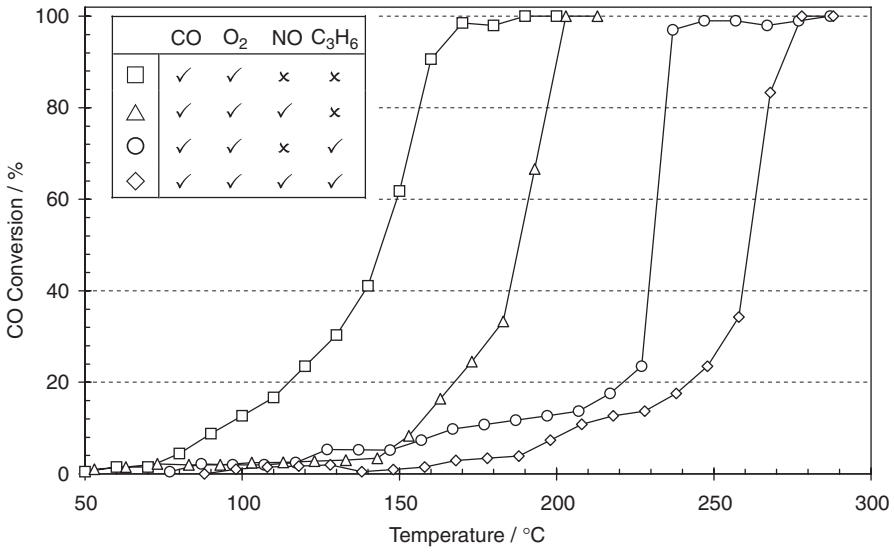

FIG. 9. CO light off under lean conditions as a function of feed composition. CO_2 and H_2O were also in the feed.

components. In this way, the influence of different components can be separated out (as far as possible) and their effect correctly accounted for in the rate equations.

Figure 10 is similar to Fig. 9, but looks at C_3H_6 oxidation. Note that C_3H_6 lights off at a higher temperature than CO as it is less reactive. As before, adding other components, viz. CO, NO and both CO and NO together, inhibits the reaction of C_3H_6, shifting the light off to higher temperature.

A complication to the above is when competing reactions occur. For example, when NO is added to the $CO + O_2$ feed, reduction of NO by CO can occur as well as CO oxidation. In this case, a rate expression for the CO–NO reaction would first be determined from experiments with CO and NO (as well as CO_2 and water), but no O_2 in the feed before considering mixtures of CO, NO and O_2. When modelling the latter, terms for O_2 inhibition may be necessary in the kinetics expression for the CO–NO reaction as well as for NO inhibition in the CO oxidation expression (as already mentioned earlier). Simultaneous reaction of C_3H_6 and CO can be handled in a similar way.

The two figures discussed so far show data measured under lean conditions, i.e. with excess O_2. Under rich conditions, there are two further complications. Firstly, it is no longer possible to completely oxidise all the CO and C_3H_6 present, so other reactions, such as partial oxidation and steam reforming of hydrocarbons and the water gas shift reaction, need to be considered. Secondly, there is competition for O_2 between the different oxidation reactions and the

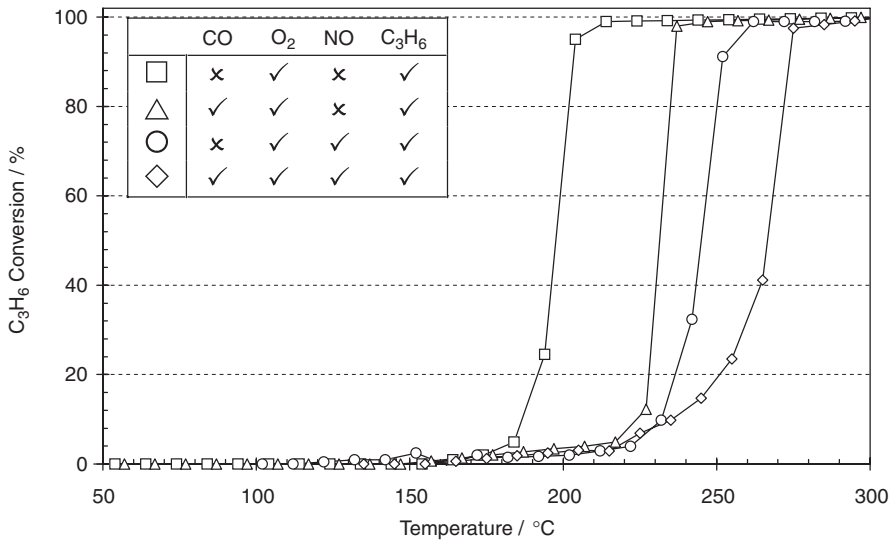

FIG. 10. C_3H_6 light off under lean conditions as a function of feed composition. CO_2 and H_2O were also in the feed.

exact selectivity to different oxidation reactions depends critically on the kinetics. These two points are discussed more fully later. Again, by careful choice of experiments, it is possible, to some extent, to study these reactions in isolation. For example, the kinetics for total oxidation of C_3H_6 can be fixed using data measured under lean conditions, before considering rich data for modelling partial oxidation and steam reforming.

Microreactor data for C_3H_6 under rich conditions are shown in Fig. 11. In this example, it is very easy to distinguish between total oxidation and steam reforming of C_3H_6, as there is a significant temperature interval between the O_2 running out and the onset of steam reforming. However, it is not always so easy to distinguish between different reactions.

An example of simultaneous reaction of CO and C_3H_6 under rich conditions is shown in Fig. 12. As the temperature is increased, CO starts to react and the CO and O_2 conversions rise. Clearly, CO starts to react before C_3H_6, because it is more reactive. Soon the O_2 conversion reaches 100%, and the CO conversion stops rising with temperature, because there is no more O_2 available for CO oxidation. As the temperature rises further, the C_3H_6 starts to react. C_3H_6 and CO are now competing for O_2, with C_3H_6 winning out. Thus, the conversion of C_3H_6 rises, while that of CO falls off. This could be explained by the activation energy for C_3H_6 oxidation being greater than that for CO oxidation, so that the rate of C_3H_6 oxidation increases faster with increasing temperature than that of CO. Eventually, C_3H_6 conversion reaches 100%, while the CO conversion

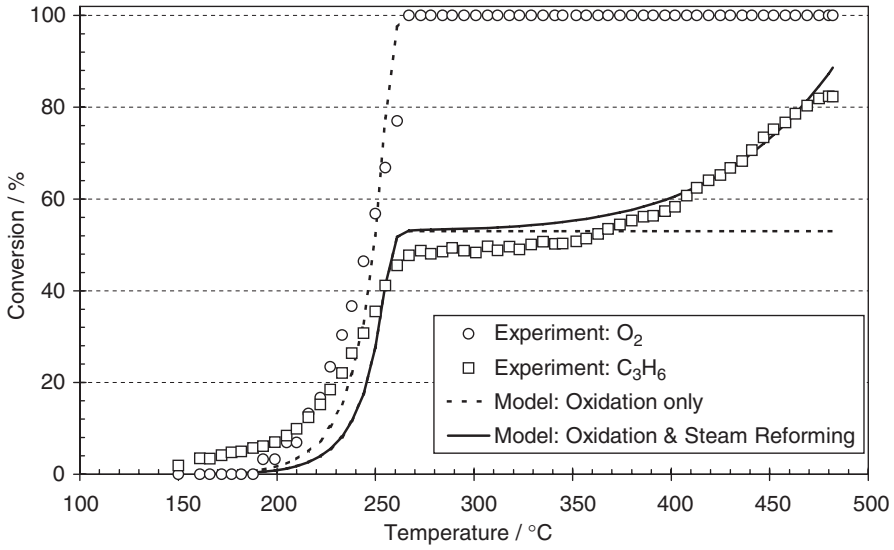

FIG. 11. C_3H_6 oxidation under rich conditions showing model predictions for a model including total oxidation only and for one with both oxidation and steam reforming together.

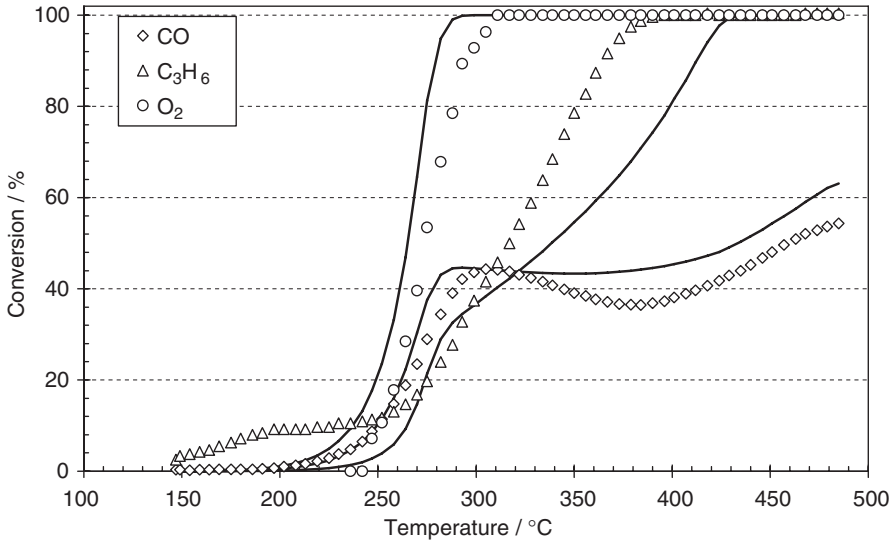

FIG. 12. Light-off curves for a rich mixture of CO, CO_2, C_3H_6, H_2O, O_2. Points are experiment, lines are simulation.

continues to fall. At still higher temperatures, the CO conversion rises again due to onset of the water gas shift reaction. Obtaining kinetics which are able to describe this competition between these finely balanced reactions over a range of feed compositions and temperatures can prove to be very challenging. Figure 12 also shows SCAT model prediction, as well as the experimental data.

An example of the importance of getting the activation energies correct when it comes to simulating competing reactions will now be discussed. Figure 13 shows a series of C_3H_6 light-off curves together with model predictions using the same C_3H_6 kinetics that worked well for the simultaneous CO and C_3H_6 oxidation shown in Fig. 12. The fit to these C_3H_6 light-off curves can be improved by decreasing the activation energy of C_3H_6 oxidation. Figure 14 shows the fit with the "improved" kinetics, which were obtained using an optimisation routine to adjust the kinetic parameters to minimise the least squares difference between experiment and simulated conversions. The fit has clearly been improved. However, when these kinetics were used on the CO and C_3H_6 oxidation data (Fig. 15), the fit was rather disappointing. The CO starts to light off as before, as the CO oxidation kinetics were unchanged. However, because the activation energy for C_3H_6 oxidation is now less than that of CO oxidation, no competition for O_2 between CO and C_3H_6 oxidation occurs. Hence, the predicted CO conversion does not fall off with increasing temperature, as observed experimentally, and C_3H_6 light off is not predicted to occur until a much higher temperature. In fact, analysis of the model shows

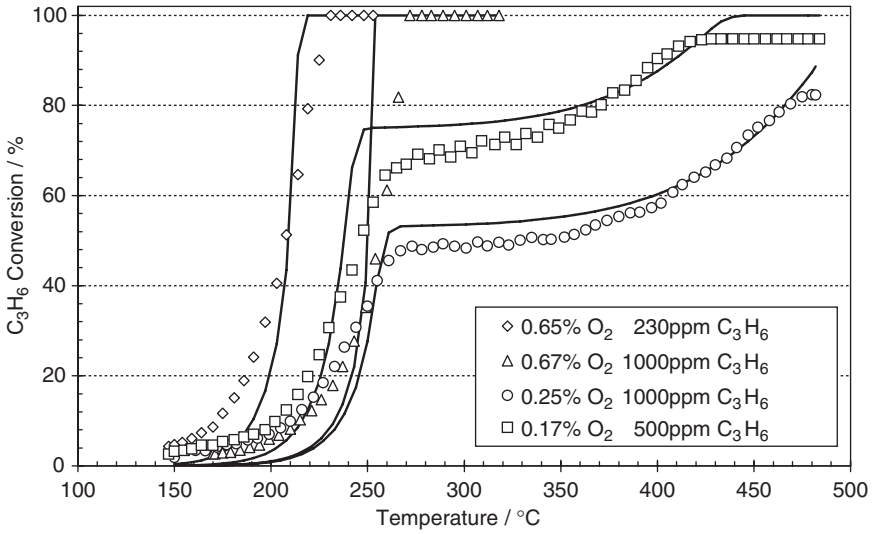

FIG. 13. C_3H_6 light-off curves with experimental data (points) and model prediction (lines) for a series of feed compositions. The kinetics are the same as used for Fig. 12.

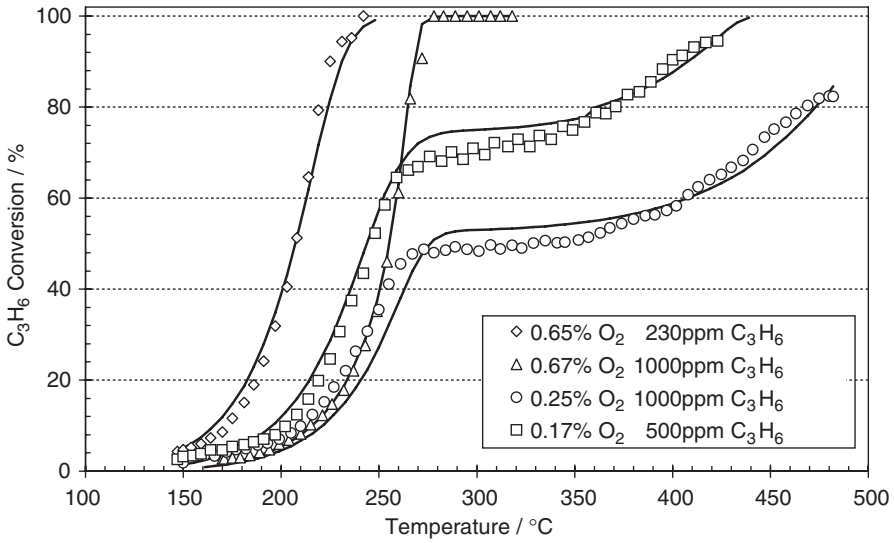

FIG. 14. The same C_3H_6 light-off curves as in Fig. 13 (points), but fitted with different kinetics (lines), which give a better fit here, but which are much less good when CO is added to the feed (Fig. 15).

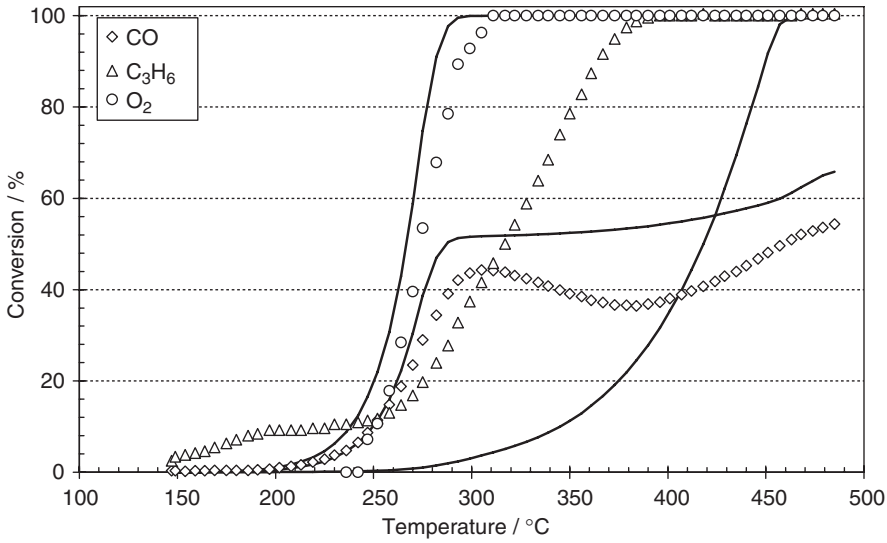

FIG. 15. The light-off data for a rich mixture of CO, CO_2, C_3H_6, H_2O, O_2 as in Fig. 12 (points), but fitted (lines) using the same C_3H_6 kinetics as Fig. 14.

that this predicted C_3H_6 conversion is solely due to steam reforming, while with the Fig. 12 kinetics it was due to total oxidation. This example, illustrates the care that needs to be taken when fixing kinetic parameters and that as more complicated gas mixtures are considered, it may be necessary to reconsider kinetics, which at first sight seemed entirely adequate with simpler gas mixtures.

So far this discussion has covered the effect of kinetics on reaction selectivity. However, it is important to realise that selectivity can also be determined by thermodynamics. It is thus necessary to write kinetics expressions that ensure the thermodynamic limitations are fulfilled for reactions where thermodynamic limitation is likely. For example, if the experiment shown in Fig. 12 were continued to higher the temperature, the CO conversion would eventually fall off with increasing temperature due to the water gas shift reaction reaching equilibrium.

As a final example of fitting SCAT data, Fig. 16 shows experimental data and SCAT model prediction for a more complicated gas mixture including CO, C_3H_6, NO and O_2. Once this sort of fit is achieved for a series of different feed compositions, the kinetics are ready to be added to the model of a monolith reactor and tested against data for a real system.

So far only steady-state kinetics have been discussed. It is also important to include a description of oxygen storage into the model. Oxygen storage components (OSC) in the catalyst, typically ceria-zirconia, serve to store and

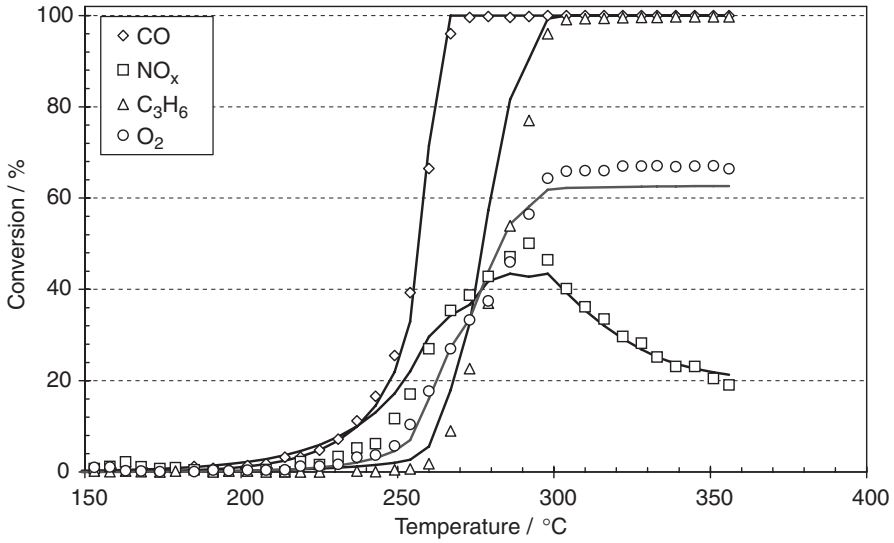

FIG. 16. Measured (points) and simulated (lines) conversions for a mixture of CO, CO_2, C_3H_6, H_2O, NO, O_2.

release oxygen to compensate for changes in reactant stoichiometry (Koltsakis and Stamatelos, 1997). When the feed gas is rich (reducing), oxygen is released to improve oxidation of CO and HC, and when the feed is lean (oxidising), oxygen is stored to improve NO_X reduction. The accessible oxygen storage capacity of a catalyst increases with temperature, up to a maximum value (Fig. 17). This is presumably related to increased mobility of oxygen in the lattice of the oxygen storage component with temperature. The importance of including a description of OSC in the model is shown in Figs. 18 and 19. These show data from a light-off experiment in which the feed was perturbed about stoichiometric composition. When OSC was not included (Fig. 18), the model gives a good prediction of light off, but at higher temperatures, it under estimates the CO, NO and O_2 conversions. The HC prediction is good throughout the whole test because HC conversion is not that sensitive to stoichiometry. Adding a description of OSC to the model (Fig. 19) gives a much improved prediction after light off.

D. MODEL VALIDATION

It is crucial that the model is able to predict catalyst performance with real vehicle data; unless tested against real data the model is only of academic interest rather than a tool of practical application. So far development of

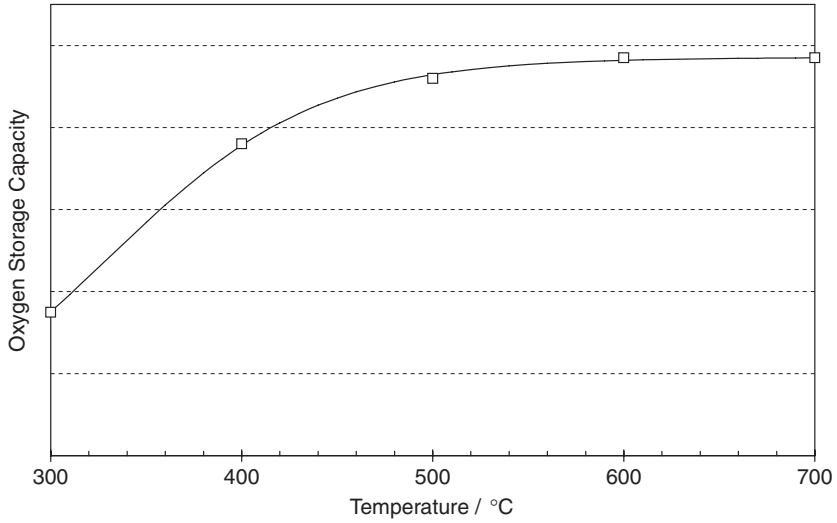

FIG. 17. Oxygen storage capacity as a function of temperature.

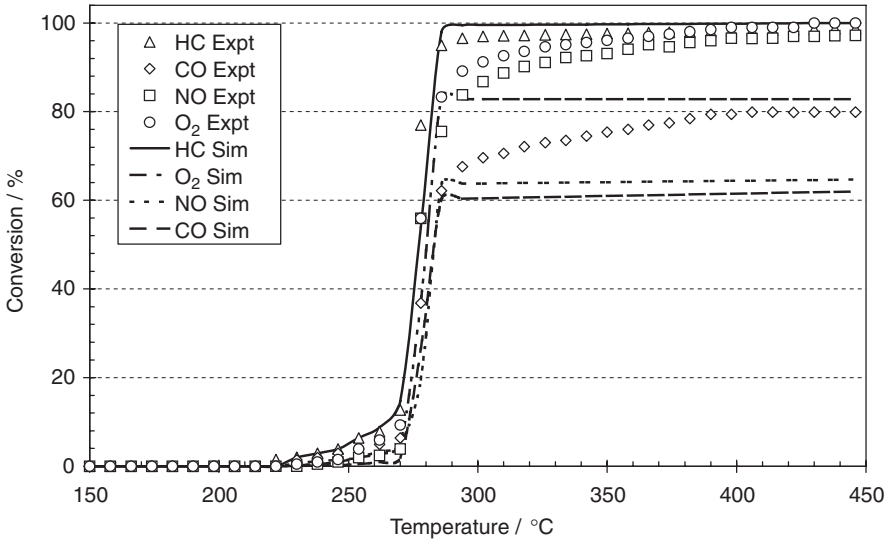

FIG. 18. Measured and simulated conversions during light off using a perturbed feed ($\lambda = 1 \pm 0.06$, frequency 0.5 Hz). OSC was *not* included in the model.

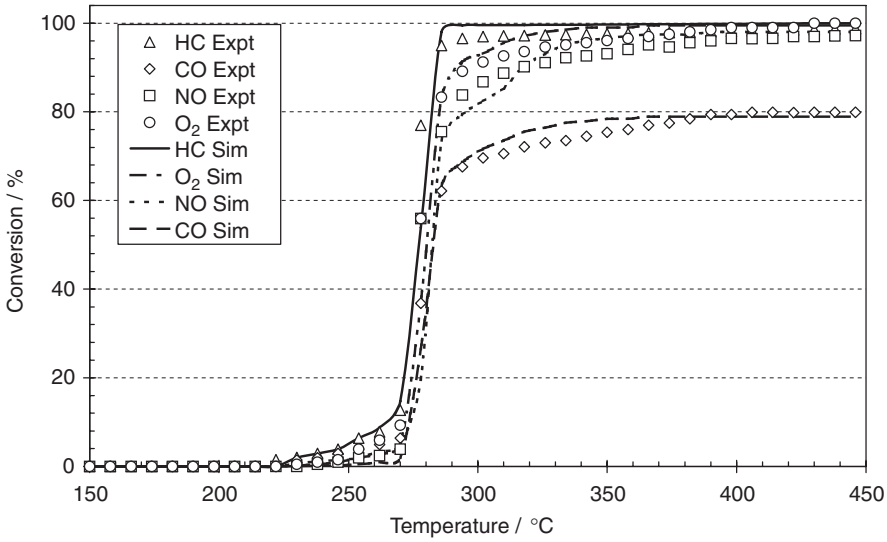

FIG. 19. Measured and simulated conversions during light off using a perturbed feed ($\lambda = 1 \pm 0.06$, frequency 0.5 Hz). OSC was included in the model.

kinetics from laboratory microreactor (SCAT) data has been discussed. The next stage of model development is to test these kinetics against real vehicle/engine data, typically measured on a rolling road or a bench-mounted engine. At this stage, the reason for any discrepancy between the model and reality needs to be determined and the model improved and re-validated accordingly.

It is important to stress that the validation process is about testing microreactor-generated kinetics against real-world vehicle/engine data, rather than about tuning the kinetics to match the data. Generally, the lab-generated kinetics are found to work well, although sometimes slight changes to the pre-exponential factor are required, for example, because the real hydrocarbons in the exhaust differ from the small selection investigated in the laboratory. Ideally, the model should be validated over all the vehicle/engine tests of interest, e.g. over both European and FTP (US) drive cycles.

An example of model validation is shown in Figs. 20–23. Predicted THC emissions for two generations of a TWC model are compared with the measured tailpipe emissions over a FTP test in Fig. 20. With the first model (labelled "Original Model"), the prediction of light off was very good, however the level of HC slip after about 400s is excessive. Clearly, this model failed the validation and it was necessary to identify the cause of the HC slip. Analysis of the model output revealed that most of the HC slipped was unreactive short chain alkanes and methane. These were being slipped because steam reforming of these hydrocarbons had not been included in the model. When these

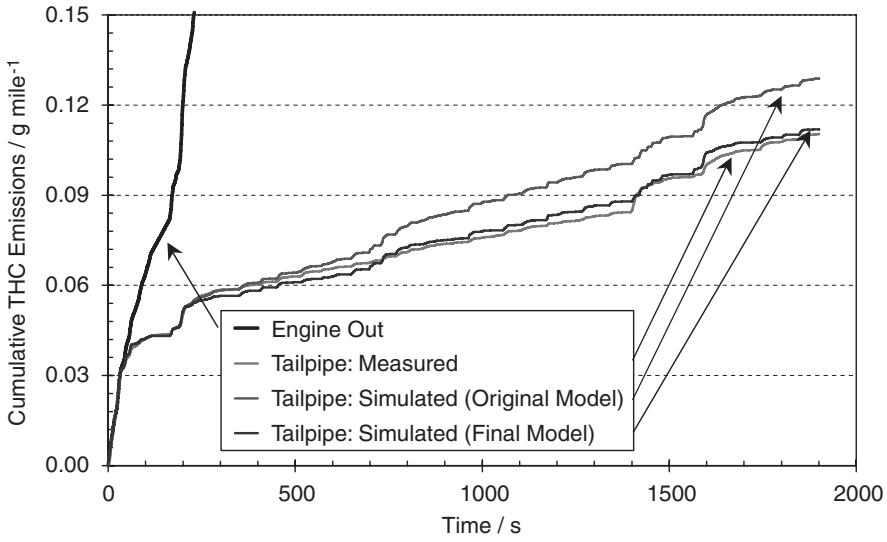

FIG. 20. Validation of a TWC model over the FTP test. Predicted THC emissions are shown for an early and an improved model.

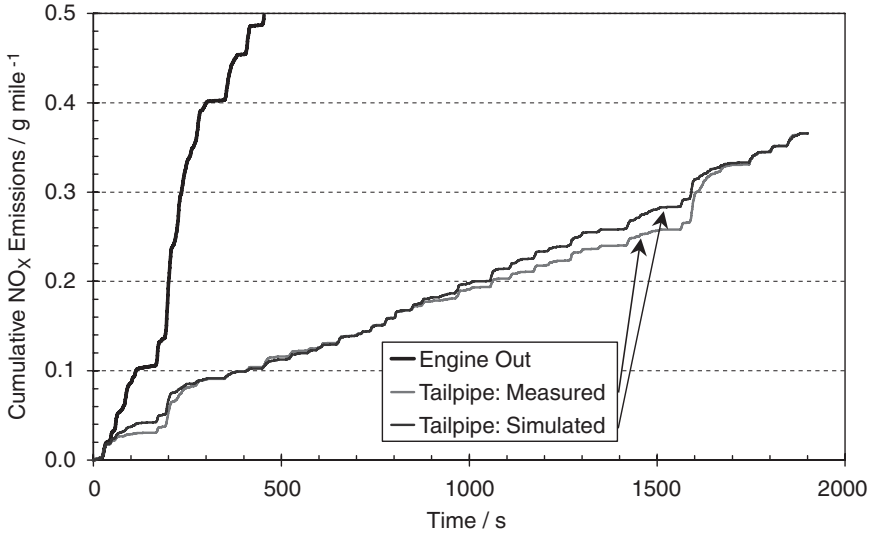

FIG. 21. Validation of a TWC model over the FTP test for NO_X emissions.

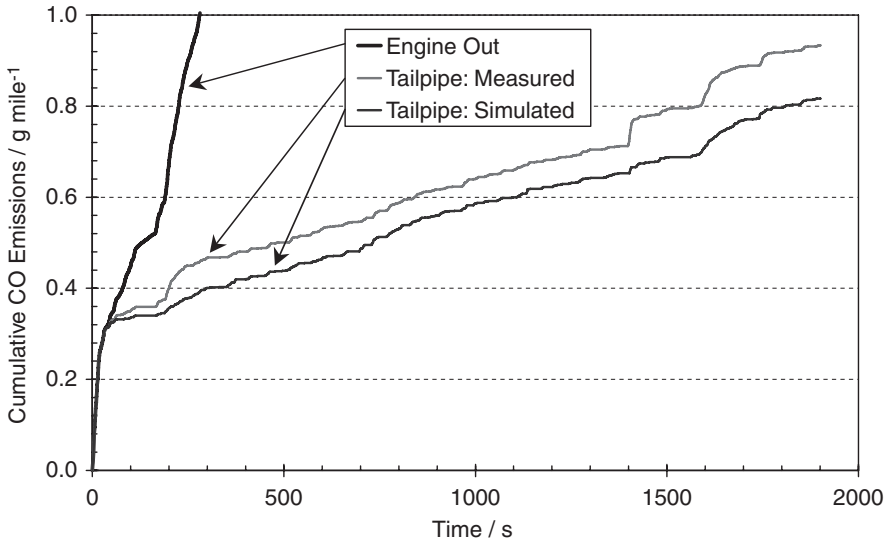

FIG. 22. Validation of a TWC model over the FTP test for CO emissions.

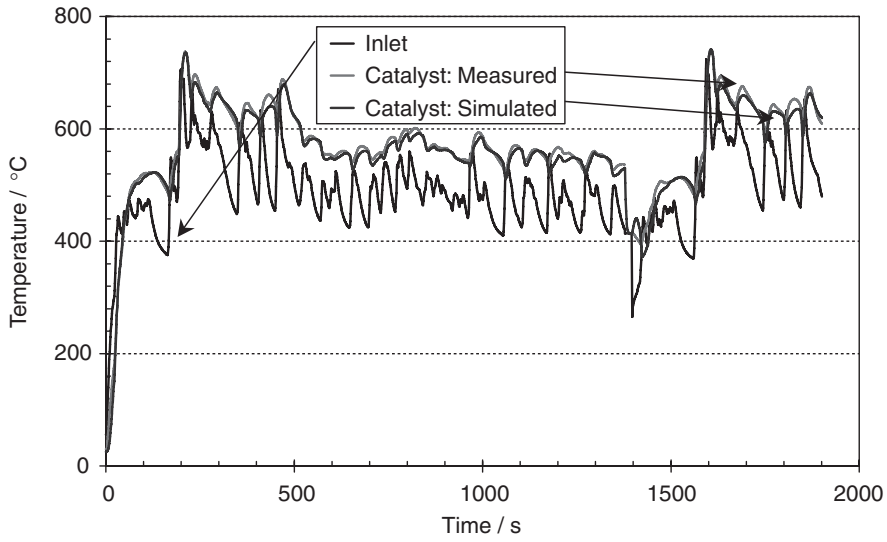

FIG. 23. Validation of a TWC model over the FTP test for temperature. Catalyst temperatures are measured 25 mm from the front face of the catalyst.

reactions were added (''Final Model'' in the figure), a much better agreement between measured and simulated emissions was obtained. In general, with TWC modelling, HC is the easiest emission to reliably predict. This is believed to be because it is the least sensitive to the air–fuel ratio.

The NO_X validation plot is shown in Fig. 21. In general, NO_X is harder to predict reliably than THC. In this case, the model gives a good prediction of light off, slips too much NO_X between 900s and 1,600s, but then under predicts the breakthrough at 1,600s to join up with the measured cumulative emissions at the end of the test. Essentially, the closer the measured and simulated emissions are throughout the whole test cycle, the more confidence one can have that the model will correctly predict the effect of a system change. It is worth noting that the model predicts all the breakthroughs to be in the right place, even if the magnitude of the breakthrough is not always correct.

The CO prediction is shown in Fig. 22. The model gives a good prediction of light off, but then fails to correctly predict the size of some of the breakthroughs, particularly those at around 200s, 1,400s and 1,600s. CO has always been found to be the most difficult emission to predict correctly. The reason for this is unclear. From a practical point of view the CO prediction is less important than the THC and NO_X predictions as CO is rarely the limiting emission for meeting the legislation with gasoline engines.

Finally, predicted and simulated catalyst temperatures are compared in Fig. 23. These temperatures were measured by a thermocouple inserted into the catalyst 25 mm from the front face, as measured in the axial direction. The agreement between measurement and prediction is good, indicating that the thermal properties used in the model for the catalyst/substrate are reasonable.

V. Other (Diesel) Aftertreatment Systems

So far this review has concentrated on model development methodology, and the application of modelling to the design of systems for gasoline vehicles using TWCs. However, of increasing importance over the past decade, and also looking into the future, will be the need for modelling to address diesel emissions control. In this field, the choice of technologies is wider than for gasoline vehicles, and a number of different aftertreatment technologies are available (Johnson, 2004; Koltsakis and Stamatelos, 1997; Twigg, 2007):

(1) Diesel oxidation catalysts (DOCs), which convert CO and hydrocarbons to more benign CO_2 and H_2O, and can also convert NO to NO_2 for possible downstream use or be used to generate higher temperatures from the

oxidation of post-injected hydrocarbon, again for downstream use. Under some circumstances a DOC can also lead to some NO_X reduction.

(2) Urea/ammonia SCR, in which a reductant, usually urea solution (Adblue, 32.5% urea (BASF, 2003)), is injected into the exhaust stream for reduction of NO_X to N_2 and H_2O.

(3) Lean NO_X trap (LNT), in which NO_X is stored on the catalyst and then the catalyst regenerated intermittently using engine control.

(4) Diesel particulate filters (DPF), which remove particulate from the exhaust stream. They can also be coated with catalyst, e.g. DOC, LNT or SCR, to enable removal of gaseous pollutants in the same system component.

Clearly with so many systems available, and tightening diesel legislation demanding a combination of various technologies, it is important to be able to design the most efficient solution. Examples of ways in which these aftertreatment technologies can be combined are shown in Fig. 24, however this is certainly not exhaustive and many other system ordering arrangements and combinations can be imagined. Furthermore, in addition to the aftertreatment technologies described, engine control strategies are also important, and

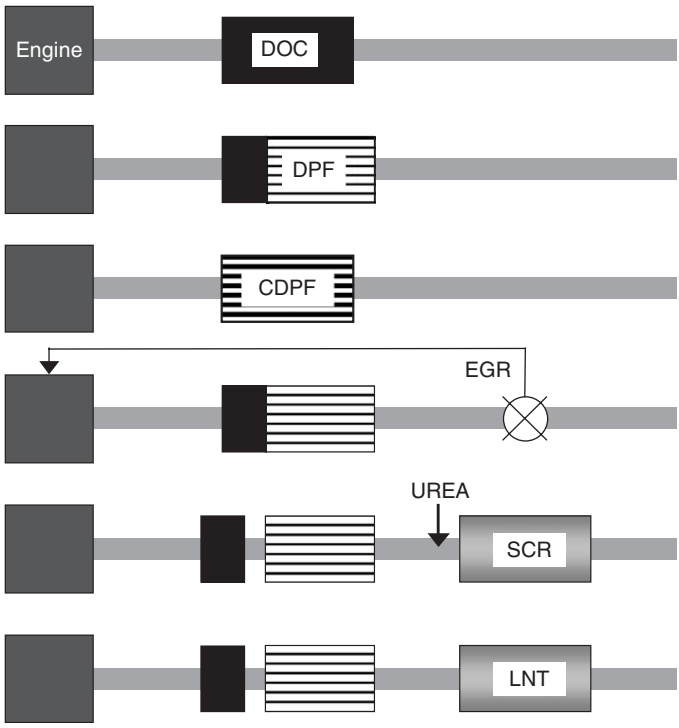

FIG. 24. Schematic diagram showing examples of possible aftertreatment systems.

systems such as exhaust gas recirculation (EGR) can be incorporated into the system design; in EGR some of the exhaust gas is recirculated into the engine intake, reducing the oxygen content and therefore the NO_X formed in the engine cylinder (Stone, 1999). With so many options and design parameters, modelling can play a critical part in diesel aftertreatment system design and optimisation.

In the following sections, the application of modelling to diesel aftertreatment will be addressed. However, given that these diesel models are developed using a similar approach and methodology to the TWC models, the emphasis in these sections will be on application of the models to system design and understanding.

A. Diesel Oxidation Catalysts

DOCs are important for reducing the emissions of CO and hydrocarbons from diesel vehicles (Clerc, 1996). Furthermore, these catalysts are active for the oxidation of NO to NO_2, which can be used in downstream systems, such as SCR and filters, where NO_2 concentration can be key to the total system performance. Modelling can play a role in designing optimum systems for CO, HC and NO oxidation.

In addition, DOCs are also capable of reducing NO_X, under certain conditions. Early work on these "lean NO_X catalysts" concentrated on Cu/ZSM-5 catalysts (Amiridis *et al.*, 1996; Walker, 1995), but platinum (Amiridis *et al.*, 1996; Burch and Millington, 1995) and silver (Breen and Burch, 2006) -based catalysts, with better hydrothermal resistance than the zeolite systems, are also available. Unfortunately, NO_X reduction under lean conditions only occurs over a narrow temperature range and therefore modelling can aid in optimisation of the catalyst and emissions system.

Because of the lean NO_X reduction function of these catalysts, it is important to include not only the oxidation reactions

$$\mathrm{CO} + \tfrac{1}{2}\mathrm{O_2} \rightarrow \mathrm{CO_2} \qquad \text{CO oxidation}$$

$$\mathrm{C}_x\mathrm{H}_y + \left(x + \frac{y}{4}\right)\mathrm{O_2} \rightarrow x\mathrm{CO_2} + \left(\frac{y}{2}\right)\mathrm{H_2O} \qquad \text{Hydrocarbon oxidation}$$

$$\mathrm{NO} + \tfrac{1}{2}\mathrm{O_2} \rightleftharpoons \mathrm{NO_2} \qquad \text{NO oxidation (reversible)}$$

but also NO reduction reactions

$$\mathrm{C}_x\mathrm{H}_y + \left(2x + \frac{y}{2}\right)\mathrm{NO} \rightarrow \left(x + \frac{y}{4}\right)\mathrm{N_2} + x\mathrm{CO_2} + \left(\frac{y}{2}\right)\mathrm{H_2O} \qquad \text{NO reduction by hydrocarbon}$$

in a model of a DOC for system simulation.

Diesel exhaust consists of a complex mixture of hydrocarbons (Wajsman *et al.*, 1996) with different reactivities and mass transport propensities. Figure 25 compares the reactivities of some hydrocarbons typically found in diesel exhaust. As with TWCs (Section IV.B), it is desirable to include a small selection of representative hydrocarbons in a DOC model to emulate the reactivity and transport properties of the real exhaust.

As discussed for TWC models (Section II), a DOC model can be used for catalyst sizing and system design. Figure 26 shows a validation plot comparing model prediction with measured data over the ESC (European Stationary Cycle); excellent agreement is observed. Good agreement has also been obtained with this model over other test cycles (York *et al.*, 2005).

Further functionality can be added to the DOC by the incorporation of a hydrocarbon storage component, typically a zeolite, to the catalyst formulation. This serves to trap hydrocarbon in the exhaust from engine start-up, when the temperature of the catalyst is too low for oxidation reactions to proceed at the required rate. This stored hydrocarbon is later released as the temperature increases, ideally at a temperature at which oxidation to CO_2 can occur. The overall result is that hydrocarbon slip is reduced even when the system is cold at start up, resulting in much lower total emissions over the drive cycle.

It is thus necessary to include a description of the thermodynamics and kinetics of hydrocarbon storage in a model of such a DOC. Typically, we have based this on hydrocarbon breakthrough experiments. In this experiment, hydrocarbon in an inert carrier is passed over an outgassed DOC core sample.

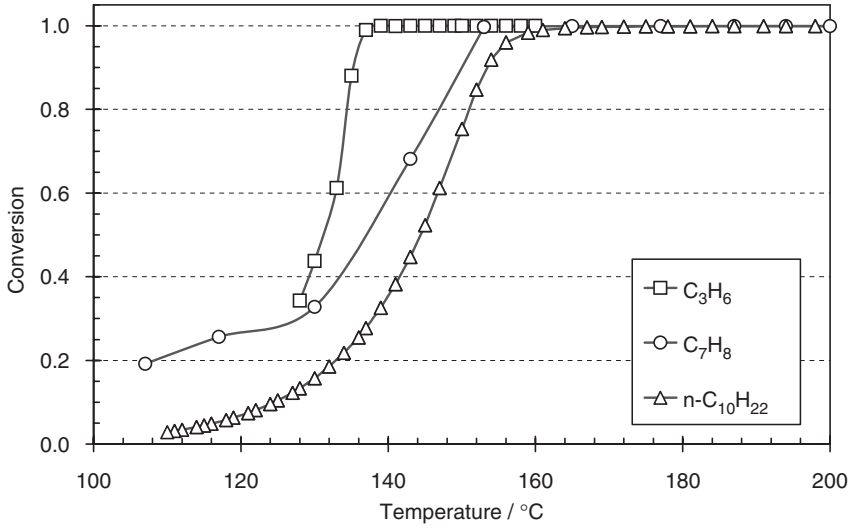

FIG. 25. SCAT light off comparison of the activity of different hydrocarbons for oxidation over a Pt-based DOC. All hydrocarbons were present at the same concentration on a C_1 basis.

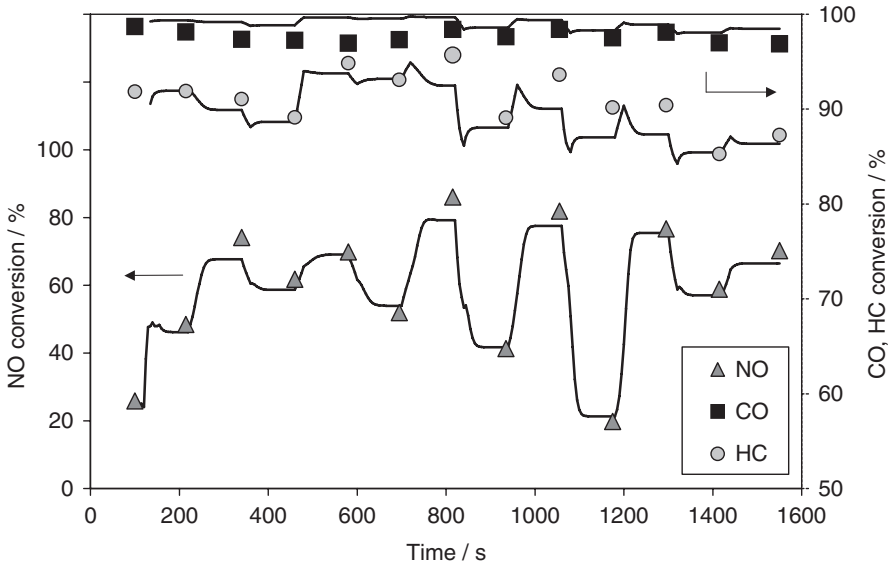

FIG. 26. Modelled (lines) and measured (points) component conversions for a DOC over the ESC (European Stationary Cycle). Measured data for a bench mounted 10 L, 210 kW turbocharged engine.

Initially, all the hydrocarbon is adsorbed on the core and none is observed at the outlet. Once the core is saturated, hydrocarbon breakthrough is observed. Example breakthrough curves for two temperatures are shown in Fig. 27. The amount of hydrocarbon adsorbed is given by the area above the breakthrough curve (after correction for the residence time of the reactor). By conducting experiments with different hydrocarbon concentrations and at different temperatures, the temperature and concentration dependency of the amount stored can be determined and hence isotherms generated.

Typically, the isotherms can be fitted to a Langmuir isotherm (Fig. 28), where the amount stored is given by

$$Q_{\mathrm{Equil,i}} = Q_{\mathrm{Sat,i}} \frac{bC_{\mathrm{si}}}{1 + bC_{\mathrm{si}}} \tag{6}$$

The temperature dependence of the constant, b, is given by the Van't Hoff relationship, viz.

$$b_{\mathrm{i}} = b_{\mathrm{i,0}} \exp(-\Delta H_{\mathrm{ads,i}}/RT) \tag{7}$$

where

b_{i}	thermodynamic equilibrium constant for adsorption of i	$\mathrm{m^3/mol}$

$b_{i,0}$	thermodynamic equilibrium constant of i at infinite temperature	m^3/mol
C_{si}	concentration of species i in the solid phase	mol/m^3
$Q_{Equil,i}$	the amount of i adsorbed at equilibrium per unit mass of washcoat	mol/kg
$Q_{Sat,i}$	the maximum amount of i that can be adsorbed per unit mass of washcoat	mol/kg
$\Delta H_{ads,i}$	heat of adsorption of i	J/mol

The thermodynamics of adsorption of a given species are thus characterised by $b_{i,0}$ and $\Delta H_{ads,i}$. By fitting the breakthrough curves, expressions for the kinetics of adsorption/desorption can be developed; Fig. 27 shows simulated, as well as measured, breakthrough curves.

An example of the application of this DOC model is shown in Figs. 29 and 30. The original system used a 300/8 substrate. There was interest in knowing if the emissions would be improved if the substrate was changed to a 400/4.5, and whether the advantage would still be maintained if the length were reduced by 10%; this length was predicted to give the same backpressure as the original system. Predicted CO emissions are shown in Fig. 29. Changing the substrate from a 300/8 to a 400/4.5 is predicted to result in earlier light off, due to reduced thermal mass, and reduced breakthrough after light off, due to improved mass transfer. Reducing the length by 10% does not, of course, affect the light off, but results is greater breakthrough after light off, with the CO

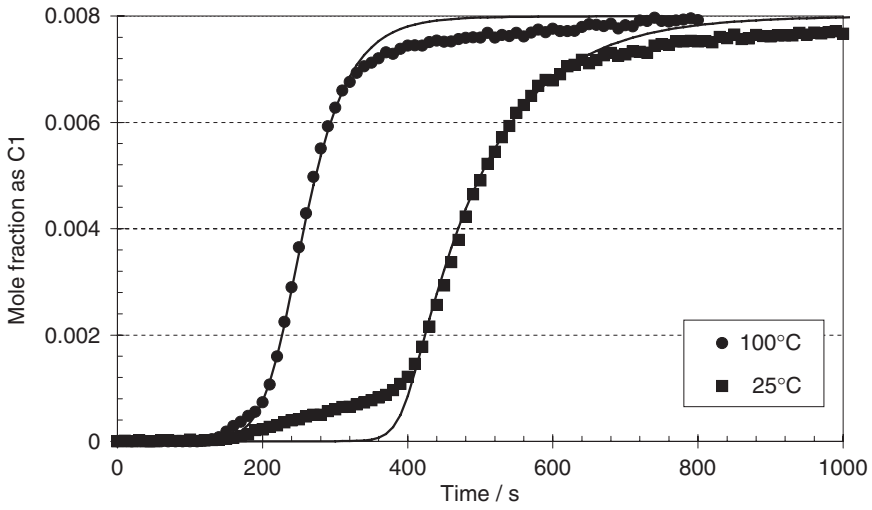

FIG. 27. Iso-octane (2,2,4-trimethylpentane) breakthrough curves on a DOC core sample. Measured (points) and simulated (lines) data are shown for two temperatures.

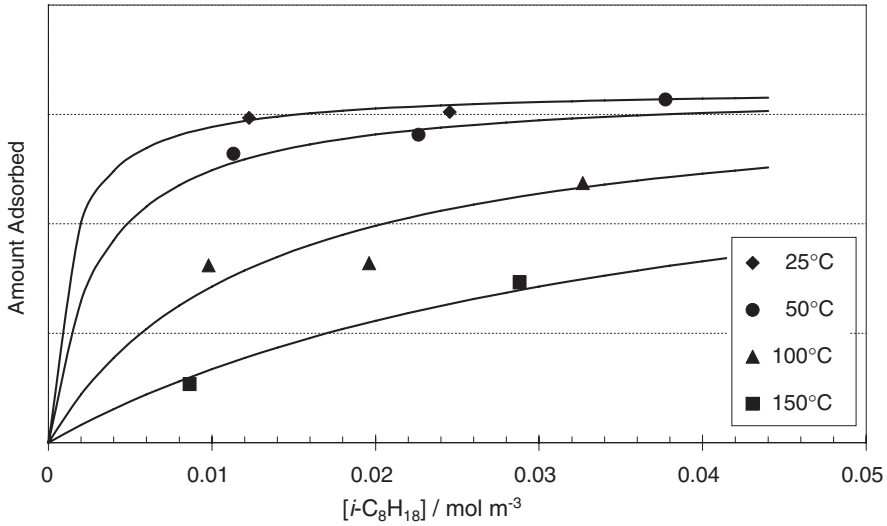

FIG. 28. Iso-octane adsorption isotherms on a DOC core sample. Points measured, lines fit to Langmuir isotherm.

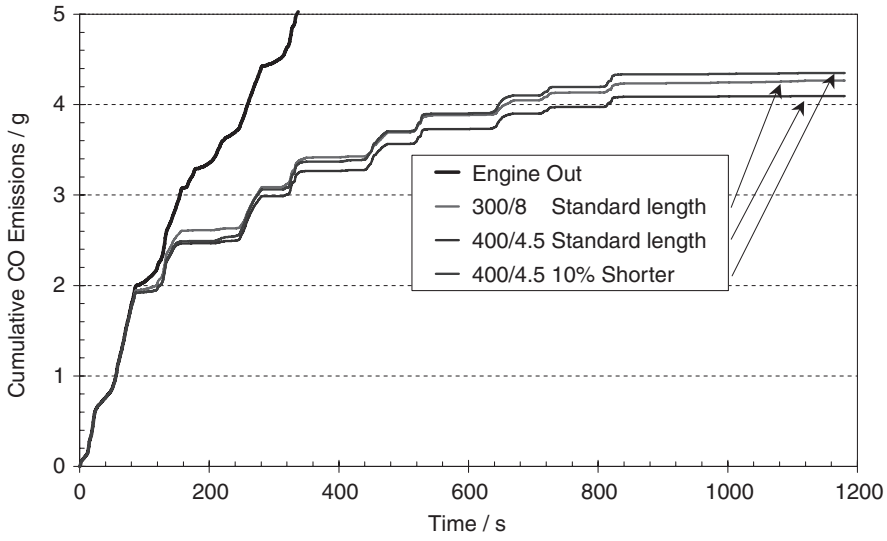

FIG. 29. Predicted effect of substrate type and length on CO emissions over the European test cycle for a Pt-based DOC containing a HC storage component.

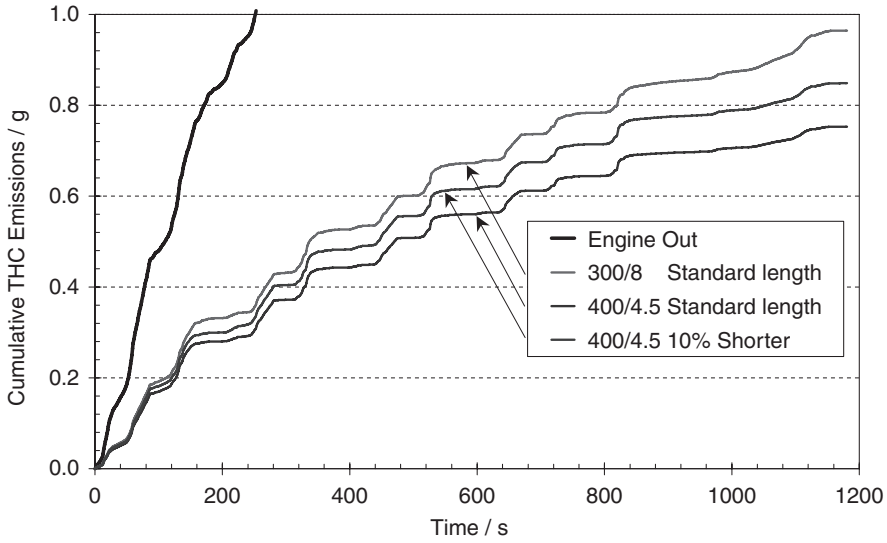

FIG. 30. Predicted effect of substrate type and length on THC emissions over the European test cycle for a Pt-based DOC containing a HC storage component.

emissions at the end of the test predicted to be higher than with the original system.

The corresponding THC prediction is given in Fig. 30. Storage of hydrocarbon in the zeolite in this formulation means that the predicted tailpipe emissions are below the engine out from time zero. Hence, catalyst light off is unimportant for THC emissions in this case. The substrate, however, still has an effect on breakthrough after light off. Thus changing the substrate from a 300/8 to a 400/4.5 results in lower emissions, due to improved mass transfer. Reducing the catalyst length by 10% is predicted to increase HC breakthrough, but, unlike the CO, the emissions at the end of the test are still lower than for the original system. It is worth noting that the substrate has a bigger effect on THC than CO emissions. This is because hydrocarbons have a greater molecular mass than CO, and so their conversion is more susceptible to mass transfer limitation, and hence more sensitive to substrate cell density.

B. AMMONIA SCR

Urea/ammonia SCR, in which NO_X is reduced by ammonia, typically introduced as an aqueous urea solution sprayed into the exhaust stream upstream of the catalyst, is one technology that is being seriously considered by

many engine/vehicle manufacturers to meet future tight NO_X emissions legislation. In addition, when combined with filter technology, SCR can provide a way to reduce both particulate matter (PM) and NO_X emissions; for example the SCRT® system (Walker *et al.*, 2000) shown in Fig. 31.

Typical catalysts for SCR include supported vanadia, and iron or copper supported on zeolite. Here the application of a model to the design and understanding of vanadia catalyst systems is presented. Over the vanadia-based catalyst system, a Rideal–Eley approach has been adopted by most workers in the field, in which the first step is ammonia adsorption on the catalyst. This stored ammonia can then either react with NO_X or be desorbed. Some important contributions to the SCR modelling literature are Andersson *et al.* (1994), Lietti and Forzatti (1994), Dumesic *et al.* (1996), Lietti *et al.* (1997), Maurer *et al.* (1999), Kleemann *et al.* (2000), Nova *et al.* (2000), Koebel *et al.* (2001), Nova *et al.* (2001), Forzatti (2001), York *et al.* (2004) and

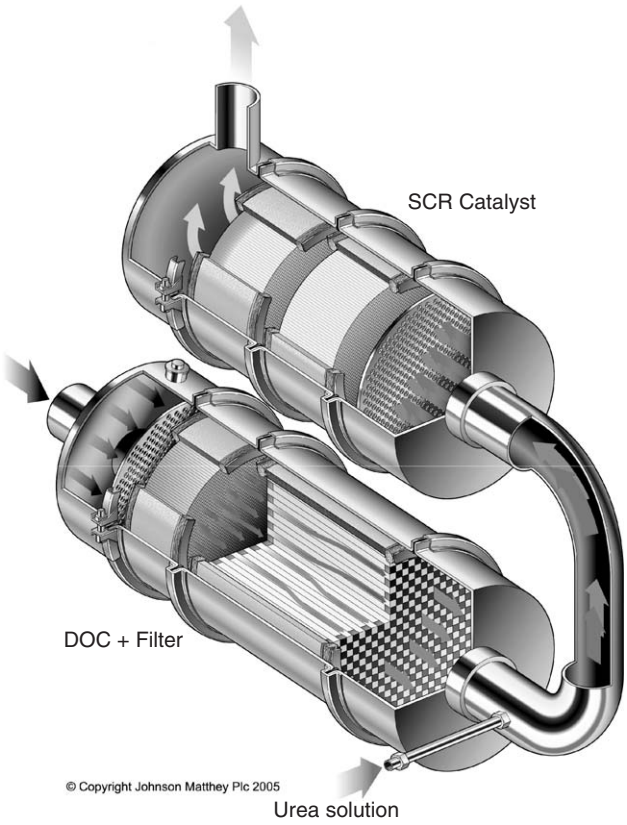

FIG. 31. Schematic diagram showing the SCRT® system for removing PM and NO_X.

Chatterjee *et al.* (2006). The most important reactions for consideration in the model are

$4NH_3 + 4NO + O_2 \rightarrow 4N_2 + 6H_2O$	SCR reaction of NO
$4NH_3 + 2NO_2 + O_2 \rightarrow 3N_2 + 6H_2O$	SCR reaction of NO_2
$2NH_3 + NO + NO_2 \rightarrow 2N_2 + 3H_2O$	SCR reaction of $NO + NO_2$
$4NH_3 + 3O_2 \rightarrow 2N_2 + 6H_2O$	Oxidation of NH_3 to N_2

Urea decomposition/hydrolysis to ammonia may also be rate limiting under very specific conditions, but is not considered in this discussion, i.e. conversion of urea to ammonia is considered to be fast.

$(NH_2)_2CO \rightarrow NH_3 + HNCO$	Urea decomposition
$HNCO + H_2O \rightarrow NH_3 + CO_2$	Hydrolysis of cyanic acid

One of the primary uses for an accurate SCR model is in the sizing of catalyst systems. The model has been shown to be accurate for the prediction of NO_X emissions and conversions, as is shown in Table I for 267 mm diameter vanadia-based catalysts of various lengths. Excellent agreement was obtained between the model and the experimental data, especially for the 17 L system.

Furthermore, in combination with the DOC model described earlier, it is possible to study the effect of NO_2, formed over the DOC, on the performance of the SCR catalyst (Table II). In the case shown, the extra NO_2 appears to have a deleterious effect on NO_X conversion. Indeed, it is now well known that too much NO_2 in the vanadia SCR catalyst results in a decrease in performance, while when optimised the NO_2 leads to a significantly improved performance (Chandler *et al.*, 2000; Gieshoff *et al.*, 2000). Therefore, it is clear to see how the models can be used for SCR system design.

Using this model, it has also been possible to probe the behaviour of the catalysts in detail. For example, experiments were conducted wherein each

TABLE I

Effect of Catalyst Length/Volume on the Overall Weighted NO_X Emissions and Conversions over 267 × 152 mm (8.5 L), 267 × 229 mm (12.75 L) and 267 × 305 mm (17 L) 400/6 SCR Catalyst Systems

Catalyst volume (L)	NO_X emissions after SCR system (g/kWh)		NO_X conversion (%)	
	Experiment	Model	Experiment	Model
8.5	1.341	1.637	82.6	78.8
12.75	–	1.108	–	85.6
17	0.796	0.794	87.6	87.7

TABLE II
THE EFFECT OF AN UPSTREAM DOC ON THE PREDICTED PERFORMANCE OF A 267 × 305 mm (17 L) 400/6 SCR CATALYST OVER THE ESC

	NO_X emissions after SCR system (g/kWh)		NO_X conversion (%)	
	Experiment	Model	Experiment	Model
Without pre-oxidation catalyst	0.796	0.794	87.6	87.7
With pre-oxidation catalyst	1.379	1.586	82.0	79.3

mode in the ESC cycle was run individually and the ammonia injection rate increased stepwise, giving an ammonia concentration from 70% to 120% of the inlet NO_X concentration in 5% steps. This was done to investigate the effect of NH_3:NO_X ratio for each ESC mode, so enabling optimisation of the NH_3 injection rate to achieve the highest possible NO_X conversion accompanied by the lowest possible NH_3 slip. Figure 32 shows the results obtained for a 267 × 305 mm, 400/6 catalyst for modes 6, 7 and 10 (medium, low and high temperature modes, respectively), and the model prediction; the catalyst was conditioned in ammonia before each run to ensure steady state ammonia coverage. For all three modes shown, very good agreement between the experimental data and the simulations was seen; similar agreement was obtained for all the remaining ESC modes. From this information it is possible to build up an understanding of the relationship between NH_3:NO_X ratio and NO_X conversion and NH_3 slip for use in system design. It was interesting to note that increasing the ammonia injection rate did not affect the NO_X conversion to any great extent in both modes 7 and 10, while the expected increase in conversion up to 100% was seen for mode 6. This effect was further investigated.

Figure 33 presents the predicted fractional ammonia coverage for the three modes at three different positions in the catalyst: viz. (1) at the front; (2) in the middle and (3) at the end. For the mid-temperature mode 6, increasing the ammonia injection rate had a marked effect on the coverage, and this was especially noticeable at the end of the catalyst bed; this leads to an increase in the reaction rate (and hence NO_X conversion (Fig. 32a)), since this is directly proportional to the ammonia coverage. At higher temperature (mode 10), the coverage did not increase markedly on increasing the injection rate, and therefore nor did the conversion; it seems that at these temperatures the ammonia is desorbed before it can react (and hence the NH_3 coverage remains close to zero). Perhaps the most interesting result was that obtained for mode 7 (low temperature), where the ammonia coverage was close to unity even at the start of the reaction with 70% injection rate. Since increasing the NH_3:NO_X ratio cannot further increase the coverage, the reaction rate (and hence NO_X conversion (Fig. 32b)) remains unchanged. This example illustrates how

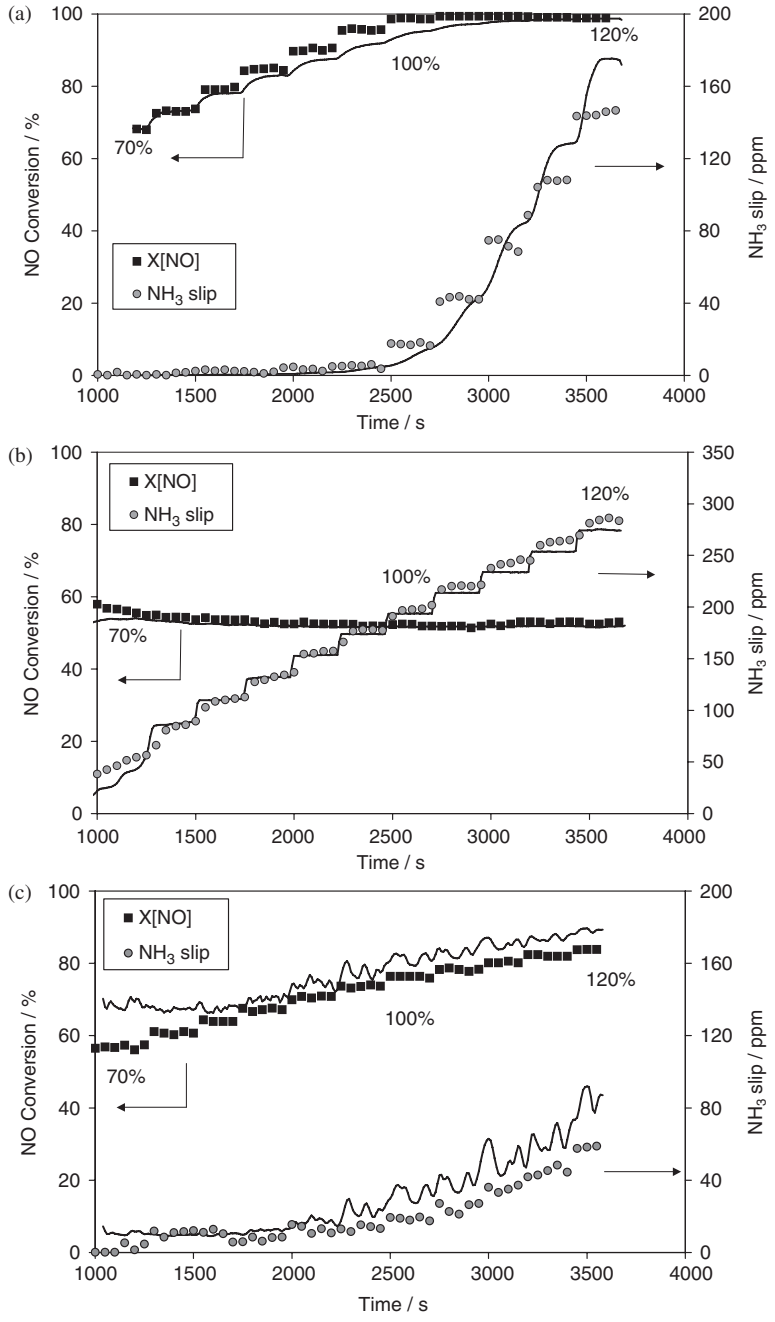

FIG. 32. Measured (symbols) and simulated (lines) NO_X conversion and NH_3 slip for (a) Mode 6 (385°C), (b) Mode 7 (285°C) and (c) Mode 10 (500°C) of the ESC cycle with progressively increasing ammonia injection rate.

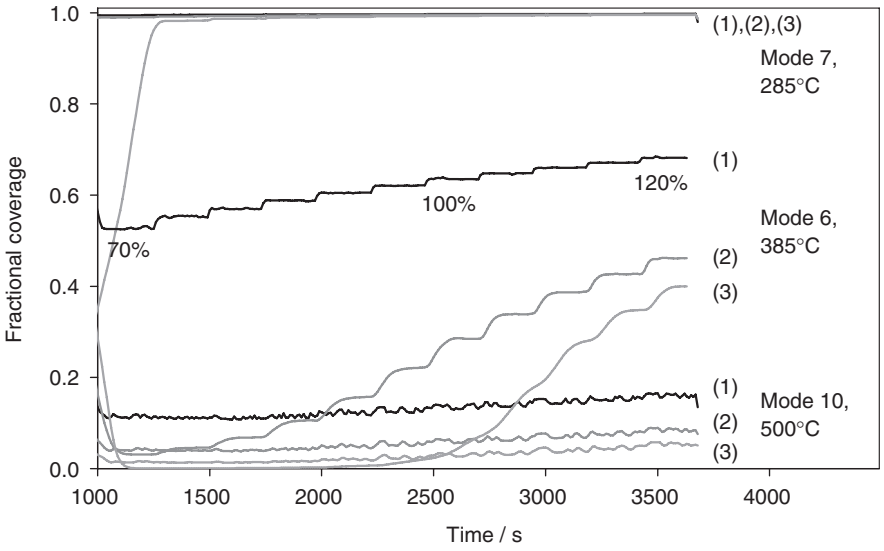

FIG. 33. Plot of calculated fractional ammonia coverage for the three ESC modes at the front (1), middle (2) and rear (3) of the catalyst brick, with progressively increasing ammonia injection rate.

modelling can be a powerful tool for rationalising and understanding complicated (and unexpected) phenomena.

C. NO_X TRAPS

Another technology under consideration for NO_X abatement in diesel vehicles is the LNT, which is also commonly called the NO_X adsorber catalyst (NAC) or NO_X storage/reduction catalyst (NSRC).

Some of the processes occurring in an LNT are somewhat similar to those in the TWC systems discussed earlier (see Section IV.B), and indeed LNT systems typically contain platinum and rhodium, as do TWCs. However, a TWC will not operate as an efficient NO_X reduction system in the presence of excess oxygen. In order to enable operation under lean conditions (e.g. diesel or gasoline direct injection engines (GDI)), a NO_X storage material is added to the catalyst: NO_X is adsorbed and stored on this material under the lean conditions usually associated with diesel exhaust, and is then released and reduced to nitrogen during a brief rich (regeneration) period of operation.

By careful choice of the storage material, catalysts with differing storage capacities and thermal properties can be designed for applications with different temperature ranges. Typical adsorber materials are the alkali and alkaline-earth metal oxides, e.g. barium, magnesium, potassium and cesium.

Clearly, when modelling an LNT it is important to include the most important processes occurring in this relatively complex catalyst system. Kinetic and experimental studies of lean NO_X trap catalysts, including those describing chemical principles, have been published previously (Brogan *et al.*, 1995; Dou and Bailey, 1998; Fekete *et al.*, 1997; Miyoshi *et al.*, 1995; Takami *et al.*, 1995). These processes can be summarised as follows:

1. Storage (Lean Operation)

Under lean (normal) conditions, NO_X is stored by oxidation of NO to NO_2, followed by NO_2 adsorption on metal oxide sites (MO) to form nitrites or nitrates (Koči and Marek, 2004; Nova *et al.*, 2004).

$2NO + O_2 \rightleftharpoons 2NO_2$	Oxidation of NO
$MO + 2NO_2 + \frac{1}{2}O_2 \rightarrow M(NO_3)_2$	Storage of NO_2 as nitrate

Understanding the storage capacity of the metal oxide material and the NO_2 adsorption rate is therefore also very important. Furthermore, oxides of sulphur in the exhaust gas, formed from combustion of sulphur compounds in the fuel (or lubricant oil), are stored in a similar manner. Since sulphates are thermodynamically more stable than the corresponding nitrate, this results in a reduction in the NO_X storage capacity of the LNT.

2. Regeneration (Rich Operation)

Eventually, after a period of normal engine operation, the LNT will become saturated and hence no longer able to store NO_X. The LNT is regenerated by subjecting it to a short period of rich operation. This reduces the nitrate, releasing NO_X, which is subsequently reduced to nitrogen, in accord with the equations below:

$M(NO_3)_2 + 3CO \rightarrow MO + 2NO + 3CO_2$	Nitrate reduction by CO
$M(NO_3)_2 + 3H_2 \rightarrow MO + 2NO + 3H_2O$	Nitrate reduction by H_2
$M(NO_3)_2 + \frac{1}{3}C_3H_6 \rightarrow MO + 2NO + H_2O + CO_2$	Nitrate reduction by HC
$NO + CO \rightarrow \frac{1}{2}N_2 + CO_2$	NO reduction by CO
$NO + 2\frac{1}{2}H_2 \rightarrow NH_3 + H_2O$	NO reduction by H_2

Due to the importance of controlled switching of the engine operation from lean to rich conditions and back again, the need to monitor the NO_X storage efficiency, and the desire to minimise the fuel penalty associated with regeneration, the design of LNT systems involves a high degree of integration with the engine management system. Modelling can significantly assist in

designing LNT system parameters, such as catalyst volume, precious metal loading and regeneration strategy.

An example of the performance of the LNT model, which has been described previously (Ahmadinejad *et al.*, 2006), for predicting NO_X removal during a pulsed switching microreactor experiment is shown in Fig. 34. In this experiment, the gas composition is switched between lean and rich (120s lean, followed by 5s rich) under isothermal conditions using a small monolith core in a microreactor. Good agreement between the model and the experimental data has been achieved. By performing a series of such experiments, it is possible to investigate the NO_X conversion efficiency over a range of temperatures. Figure 35 shows the experimental NO_X conversion (calculated from the analysis of the last three lean/rich cycles) and the simulated conversion; good agreement is observed across the whole temperature window. Similar simulations could be performed to probe the regeneration strategy of a full-sized LNT system.

The results of a modelling study looking at the effect of reducing the LNT catalyst volume on the NO_X conversion are shown in Table III. For the "original length" system, experimental data measured on a heavy-duty diesel engine was available; good agreement between measured and predicted emissions was observed. As expected, decreasing the catalyst volume leads to a decrease in predicted NO_X conversion.

The model has also been used to investigate the effect of reducing the engine out NO_X on the volume of the LNT system required to meet a set NO_X emissions level. This type of information can be used to weigh up economic

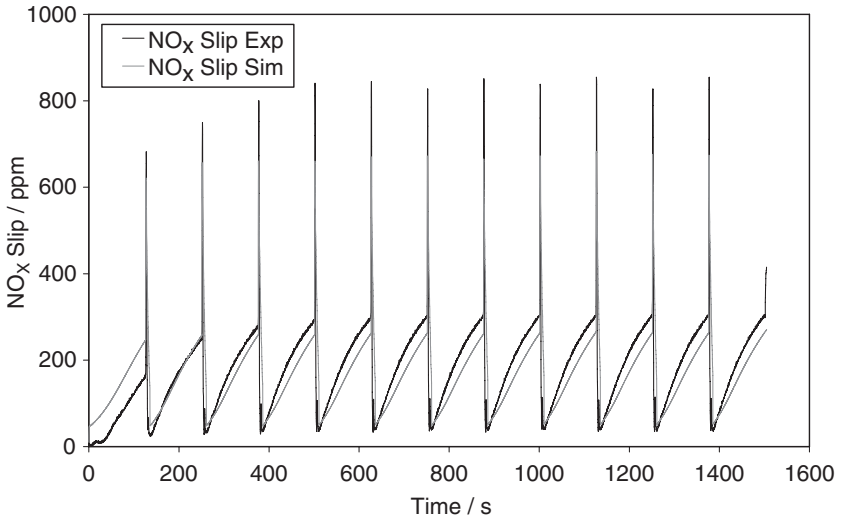

FIG. 34. Microreactor data for pulsed lean/rich cycling using an LNT at 280°C, 50 k/h, 500 ppm NO_X inlet. Experimental data in black, simulation in grey.

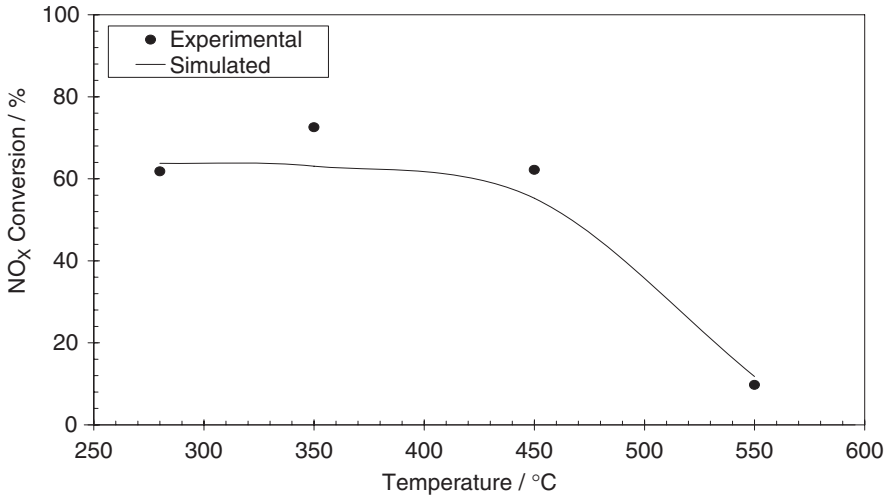

FIG. 35. Overall NO_X conversion during lean/rich cycling microreactor experiments over a range of temperatures for an LNT (50 k/h, 500 ppm NO_X inlet).

TABLE III
EFFECT OF CATALYST LENGTH ON NO_X CONVERSION OVER THE FTP CYCLE

Catalyst length	NO_X conversion (%)
Original length	68
Length reduced by 10%	62
Length reduced by 20%	57
Length reduced by 30%	51
Length reduced by 40%	45

advantages of engine re-calibration versus the size (and hence cost) of the LNT catalyst. For example, the model predicts (Fig. 36) that the same cumulative emissions can be obtained with a 16% smaller LNT, if the engine out emissions are reduced by 25%.

D. FILTERS

DPFs are important aftertreatment devices, enabling significant reduction in the emissions of PM. Typically, the filters are made of cordierite or silicon carbide materials, and can be either coated with a catalyst or left uncoated. The exhaust stream is forced to flow from one channel of the filter to an adjacent channel (see Fig. 37): the PM is filtered out by the wall of the filter.

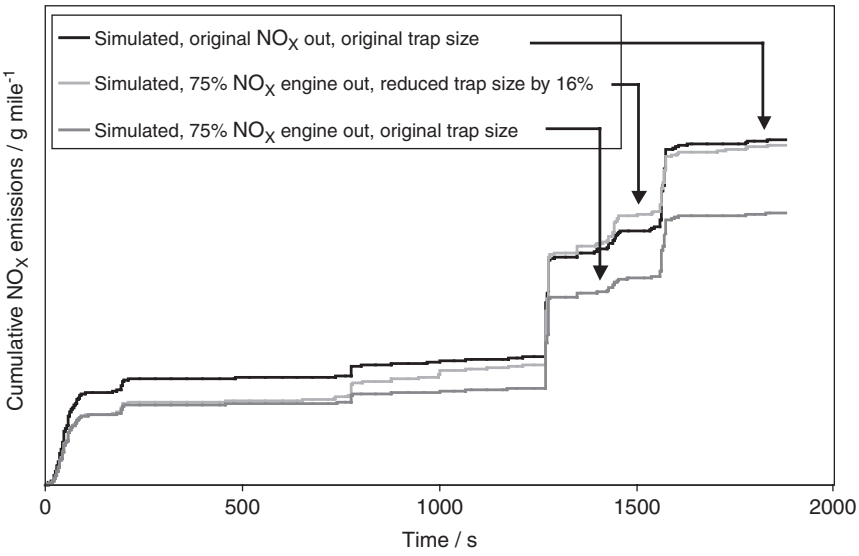

FIG. 36. Predicted effect of catalyst size and engine out NO_X on tailpipe NO_X emissions.

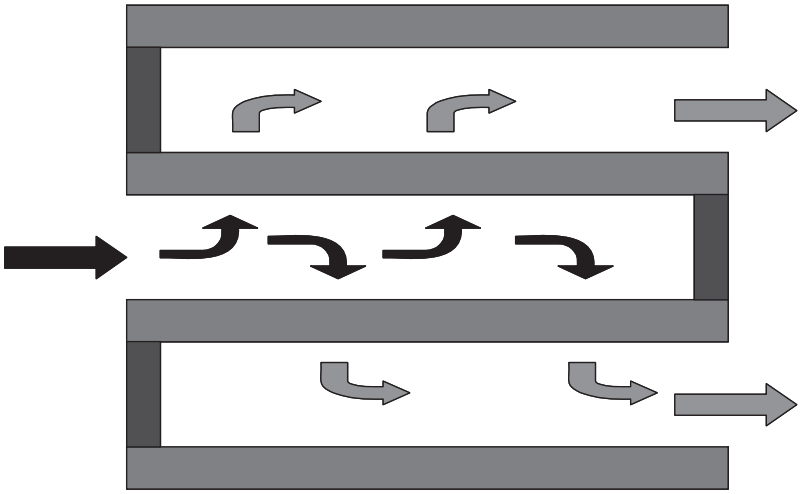

FIG. 37. Schematic showing the operating principle of a DPF.

The PM is generally removed from the filter by oxidation, either with oxygen or nitrogen dioxide, a more reactive species, as shown in the equations below:

$C + NO_2 \rightarrow CO + NO$	Soot oxidation by NO_2 to CO
$C + 2NO_2 \rightarrow CO_2 + 2NO$	Soot oxidation by NO_2 to CO_2
$C + \frac{1}{2}O_2 \rightarrow CO$	Soot oxidation by O_2 to CO
$C + O_2 \rightarrow CO_2$	Soot oxidation by O_2 to CO_2

Regeneration using nitrogen dioxide is the basis for the operation of the CRT® diesel particulate filter system (Allansson *et al.*, 2002; Cooper *et al.*, 1990).

DPFs have generated a huge amount of interest recently, and a number of research groups worldwide have concentrated on modelling their performance (Bissett, 1984; Konstandopoulos and Johnson, 1989; Konstandopoulos and Kostoglou, 2000; Konstandopoulos *et al.*, 2000, 2001, 2002; Kandylas and Koltsakis, 2002; Rumpf and Gupte, 1971; Zhang *et al.*, 2002). Filter modelling can be divided up into a number of areas, namely: (1) physical model: flow through the filter, pressure drop prediction, etc.; (2) soot accumulation and removal by oxidation; and (3) wall filtration modelling: filtration efficiency/soot capture probability in the wall and the effect of captured soot on wall porosity, etc. In addition, when the filter is coated with a catalyst layer we also need to consider: (4) gaseous component conversion, i.e. CO, HC, NO oxidation and (5) NO_2 diffusion from the catalyst in/on the filter wall back to the soot layer (so-called "back diffusion"). 1–3 and 5 have been covered extensively (Bissett, 1984; Haralampous *et al.*, 2004; Huynh *et al.*, 2003; Konstandopoulos and Johnson, 1989; York *et al.*, 2005, 2007), and are also covered in part elsewhere in this volume (Konstandopoulos *et al.*, this volume). The application of a coated filter as a gaseous emissions control device has received far less attention and will be discussed now.

In most modelling studies to date, diffusion has been ignored so that the reactant molecules simply flow with the bulk gas flow along the inlet channel and through the wall to the catalyst coating on/in the filter wall. This means that the concentrations of the reactants along the length of the inlet channel, and hence that seen by the catalyst, will be constant (when volume changes due to temperature are ignored). Such a model tends to predict reaction to occur evenly over the length of the catalyst. While this sort of model appears to perform well compared to measured data for filters evenly loaded with PGM (platinum group metal) along their length, they fail to predict the effect of PGM distribution (i.e. zoning). In these zoned systems, the filter is loaded with a higher PGM loading at the front than at the rear. Experimentally, these give improved emissions reduction compared to an evenly loaded part with the same total amount of metal. However, the "convection model" fails to predict this advantage

as the activity gain at the front of the filter is offset by the activity loss at the rear. Similarly, when an evenly loaded filter is subjected to real-world aging, often the rear of the filter experiences higher temperatures than the front (during regeneration/soot removal), leading to non-uniform aging and hence non-uniform activity gradients within the filter system; again the effect of this cannot be predicted using a model that only includes transport of reactants by convection.

With a monolith reactor, diffusion from the channels to the catalyst coated on the channel walls is the sole means by which reactants are able to reach the catalyst (Section III). It seems reasonable that a similar diffusion process occurs in a coated filter.

In a new approach to modelling catalysed DPF (CDPF) systems, transport equations have been incorporated to account for the transfer of reactants to the catalyst surface by diffusion from the bulk flow from both the gas flowing along the coated channels and the gas passing through the filter wall. With this model, the reaction zone is moved towards the front of the filter compared with the ''convection model''. Figure 38 shows hydrocarbon and NO_X concentrations as a function of axial position. It can be seen that, for example, the THC concentration drops (Fig. 38a) from its inlet value to close to zero in the inlet channel as the hydrocarbons react, but in the outlet channel a small amount of hydrocarbon is also present. This is because some of the hydrocarbons are able to pass through the wall unreacted, implying the conversion is mass transfer limited. Mass transfer limited hydrocarbon conversion has been shown earlier with monolith reactors (Section V.A). Figure 38b shows the concentration of NO and NO_2 along the length of the filter channel. Oxidation of NO to NO_2 over the catalyst coating results in a decrease in NO concentration and a corresponding rise in NO_2 concentration along the inlet channel. Along the outlet channel, the NO concentration decreases due to dilution by gas entering from the inlet channel with a lower NO concentration. For most of the length of the filter the NO concentration is higher in the outlet channel than in the inlet channel as the rate of dilution along the outlet channel is slower than the rate of NO reaction along the inlet channel.

With a good description of the mass transfer processes occurring in a CDPF now in place, it should be possible to predict the effects of PGM zoning and non-uniform aging on the performance of a CDPF. To illustrate the way in which this model can help in optimising the placement of the PGM washcoat in a CDPF systems, simulations were carried out over the European drive cycle for:

(i) Uniform PGM loading along the inlet channel (''Uniform PGM loading'').
(ii) Uniformly loaded along the front half of the inlet channel and the rear half of the outlet channel (''Front 1/2 inlet, rear 1/2 outlet'').
(iii) A higher PGM loading on the front half of the inlet channel than that on the rear half (5:1), while keeping the overall PGM levels the same as in examples i and ii (''Loaded 5:1 PGM'').

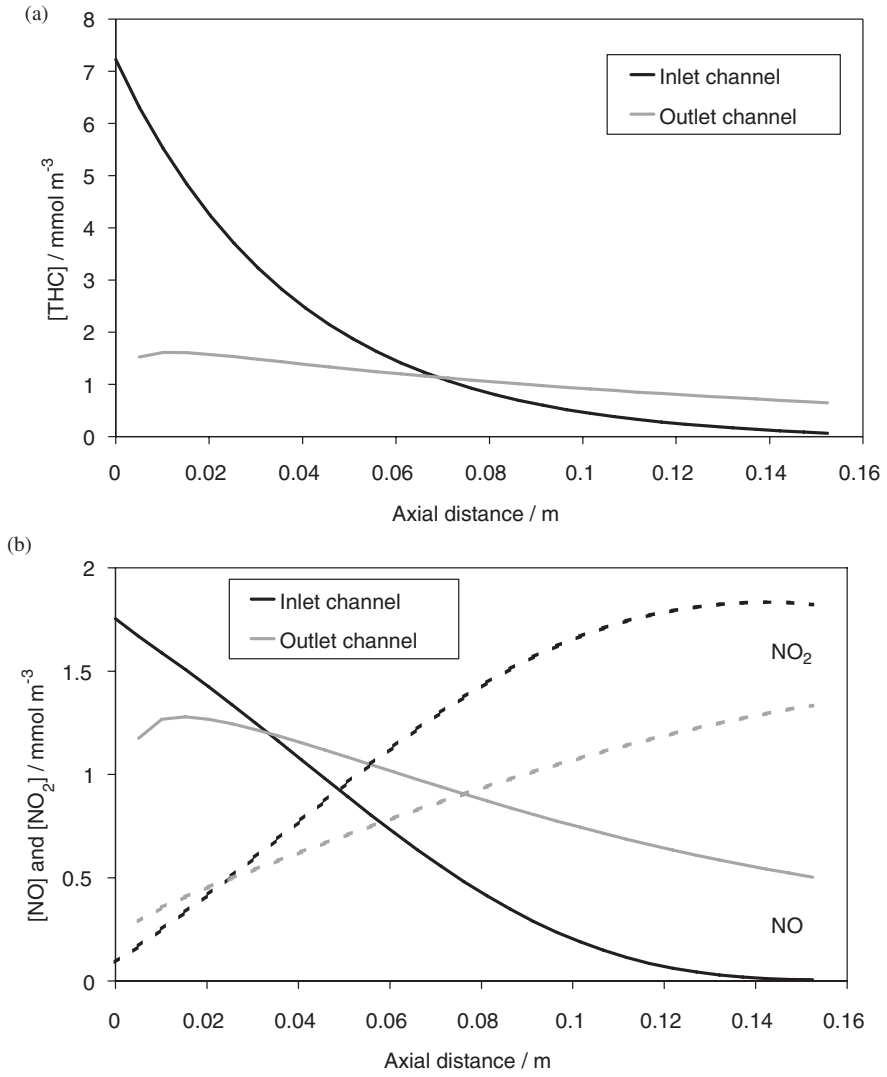

FIG. 38. Snapshot of the (a) hydrocarbon and (b) NO/NO_2 concentrations as a function of the axial distance along a catalysed filter (5.66×6 in/144×152 mm) at a temperature of 165°C.

The simulation results are shown in Fig. 39. It can be seen that lower CO and THC emissions are obtained with both the "zoned" CDPF systems, i.e. "Loaded 5:1 PGM" and "Front 1/2 inlet, rear 1/2 outlet". In the case of the "Loaded 5:1 PGM" a slightly earlier light off is observed, due to higher activity at the front of the filter (the first part to heat up), resulting in lower total

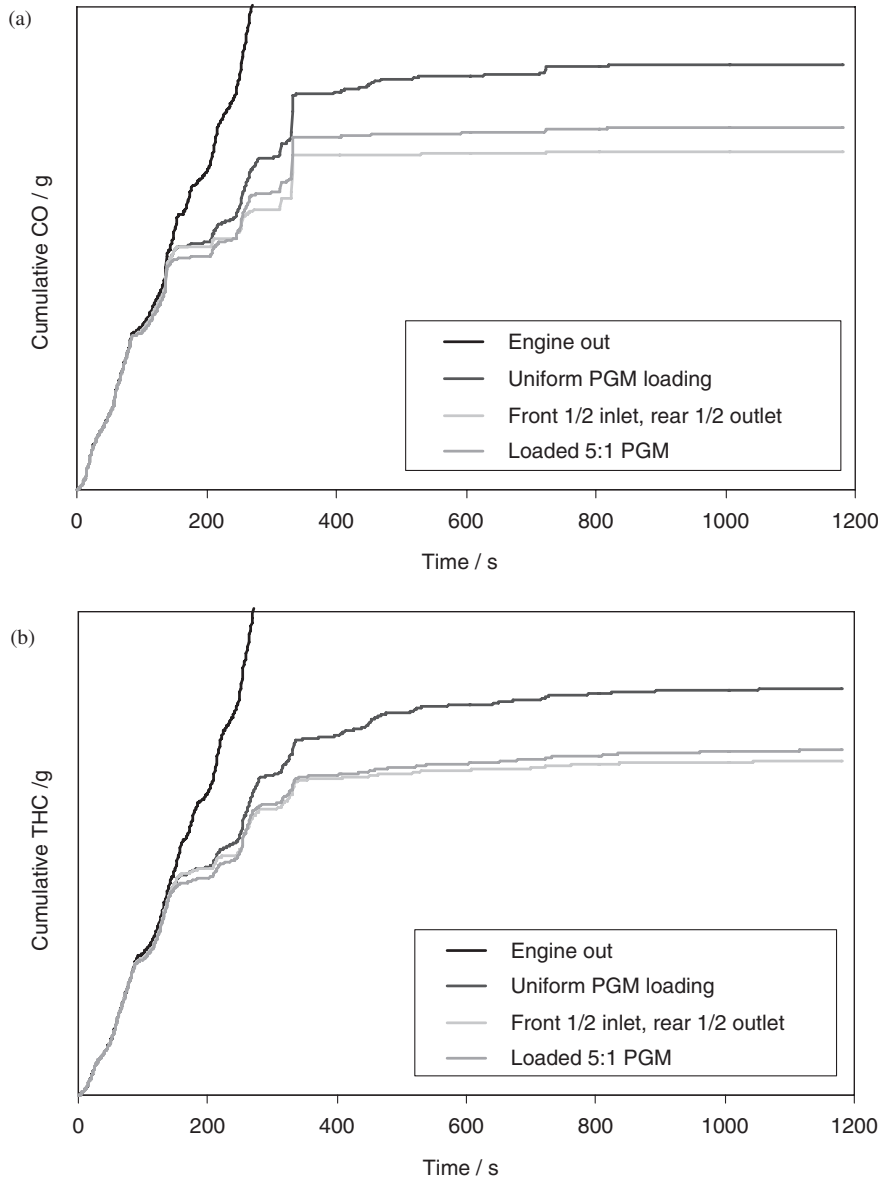

FIG. 39. Illustrative examples showing the effect of PGM distribution on the emissions of (a) CO and (b) THC over the European test cycle.

emissions. For the ''Front 1/2 inlet, rear 1/2 outlet'' system the advantage over the uniform system is due to the ability to oxidise CO and THC, which has passed into the outlet channel unreacted, over the catalyst coated onto the rear half of the outlet channel.

This illustrative study, using the new approach to CDPF emissions modelling, shows that PGM distribution can have a significant effect on emissions. In later work, with improved kinetics that more closely describe the ''real-world'' system performance, it has been shown that very great cost savings can be achieved by correctly zoning the CDPF (York *et al.*, 2008).

VI. Future Directions

Interest in computer simulation as a means of accelerating the design process for aftertreatment systems has grown rapidly in recent years and this growth is likely to continue. A few years ago, when aftertreatment was only required for gasoline engines, there was only a single product to model, viz. the TWC. With the recent introduction of emissions legislation for diesel engines, the range of emissions control technologies to model has increased to include diesel oxidation catalysts, ammonia SCR, ammonia slip catalysts, NO_X traps, particulate filters, etc. There are now many groups working on modelling these components.

In the future, aftertreatment systems are likely to become more complicated, particularly for diesel engine exhaust, as legislation becomes evermore stringent. Separate components may be required for NO_X, particulate, and CO and HC control. Alternatively, for reducing cost and packaging volume, more than one component may be combined in a single unit. This may involve coating one catalyst technology onto a filter, to control both particulate and gaseous pollutants in a single unit, or coating two (or more) different catalysts onto a single substrate, either as front and rear zones or as a series of layers (e.g. Nakanishi *et al.*, 2006) along the catalyst length. Diesel systems also frequently require some regeneration strategy, e.g. to remove soot from a filter or to regenerate a NO_X trap. Ammonia SCR requires a strategy for determining the urea injection rate. In designing such complicated systems, the number of variables to be optimised for a given system is large, as is the complexity of comparing different system types. Hence computer simulation becomes increasing useful to improve the design of the emissions system and to reduce the development time.

It is important to realise that the emissions control system does not function in isolation, but is part of a system with the engine and the rest of the vehicle/machine. There is thus interest in modelling the whole vehicle/machine (Assanis *et al.*, 2000; Fluga, 1993; Fussey *et al.*, 2001; Sahraeian *et al.*, 2004), so that the

engine calibration, emissions (Fussey *et al.*, 2001) and indeed the rest of the vehicle can be designed/optimised together.

As computers become faster, the complexity of problem that can be usefully simulated increases. Areas of interest include combining computational fluid dynamics (CFD) modelling with chemical kinetics to investigate (and hence reduce) the effect of flow maldistributions on aftertreatment system efficiency, and simulating catalyst deactivation over the lifetime of the catalyst.

In the distant future, developments in molecular modelling may enable catalyst performance/reaction kinetics to be predicted without actually making the catalyst. This would make catalyst design a real possibility. However, this is still a long way off.

ACKNOWLEDGEMENT

We would like to thank Johnson Matthey PLC for permission to publish this paper.

LIST OF SYMBOLS

[A]	concentration of species A (mol/m^3)
A_j	pre-exponential factor for reaction j (m$^{3(m+n)}$/mol$^{(m+n-1)}$/kg/s)
b_i	thermodynamic equilibrium constant for adsorption of i (m^3/mol)
$b_{i,0}$	thermodynamic equilibrium constant of i at infinite temperature (m^3/mol)
C_{gi}	concentration of species i in the gas phase (mol/m^3)
C_{si}	concentration of species i in the solid phase (mol/m^3)
C_{pg}	specific heat capacity of gas phase at constant pressure (J/kg/K)
C_{ps}	specific heat capacity of solid phase at constant pressure (J/kg/K)
E_j	activation energy of reaction j (J/mol)
H_i	heat of formation of species i (negative for exothermic reaction) (J/mol)
h	heat transfer coefficient for transport between solid and gas phases (W/m^2/K)
h_o	heat transfer coefficient for heat loss to the surroundings (W/m^2/K)
k_a,k_b,k_c	Langmuir–Hinshelwood coefficients (m^3/mol)
$k_{m,i}$	mass transfer coefficient for species i (m/s)
L	mass of catalyst per unit volume of monolith (kg/m^3)
m, n	indices in rate equation (-)
p, q	indices in rate equation (-)

$Q_{\mathrm{Equil,i}}$	the amount of i adsorbed at equilibrium per unit mass of washcoat (mol/kg)
$Q_{\mathrm{Sat,i}}$	the maximum amount of i that can be adsorbed per unit mass of washcoat (mol/kg)
r	radius of monolith (m)
R	molar gas constant (J/mol/K)
R_{i}	rate of formation of species i per unit mass of catalyst (mol/kg/s)
r_{j}	rate of reaction j per unit mass of catalyst (mol/kg/s)
S_{V}	geometric surface area (surface area of channels/volume of monolith) (m^{-1})
t	time (s)
T_{g}	temperature of the gas phase (K)
T_{s}	temperature of solid (monolith) (K)
T_{Surr}	temperature of surroundings (K)
v	mean velocity of gas in channel (m/s)
z	axial distance (m)
$\Delta H_{\mathrm{ads,i}}$	heat of adsorption of i (J/mol)
ε	open frontal area of monolith (-)
$\varepsilon_{\mathrm{WC}}$	washcoat porosity $\times$ volume of washcoat/solid volume of monolith (-)
λ	thermal conductivity of coated monolith (W/m/K)
ρ_{g}	density of gas ($\mathrm{kg/m^3}$)
ρ_{s}	solid density of monolith ($\mathrm{kg/m^3}$)

ABBREVIATIONS

CDPF	catalysed diesel particulate filter
DOC	diesel oxidation catalyst
DPF	diesel particulate filter
EGR	exhaust gas recirculation
ESC	European stationary cycle; test cycle for heavy-duty diesel engines
FTP	Federal Test Procedure; a standard US drive cycle
HC	hydrocarbon
LNT	lean $\mathrm{NO_x}$ trap
OSC	oxygen storage component/capacity
PGM	platinum group metal
PM	particulate matter
SCAT	simulated catalyst activity test, i.e. a microreactor test
SCR	selective catalytic reduction
THC	total hydrocarbon
TWC	3-way catalyst

REFERENCES

Ahmadinejad, M., Watling, T. C., York, A. P. E., Walker, A. P., Chen, H.-Y., Hess, H. S., and Cox, J. P. *SAE* 2006-01-3445 (2006).

Allansson, R., Blakeman, P. G., Cooper, B. J., Hess, H. S., Silcock, P. J., and Walker, A. P. *SAE* 2002-01-0428 (2002).

Amiridis, M. D., Zhang, T., and Farrauto, R. J. *Appl. Catal. B: Environ.* **10**, 203 (1996).

Andersson, S. L., Gabrielsson, P. L. T., and Odenbrand, C. U. I. *AIChE J.* **40**, 1911 (1994).

Ansell, G. P., Bennett, P. S., Cox, J. P., Frost, J. C., Gray, P. G., Jones, A. -M., Rajaram, R. R., Walker, A. P., Litorell, M., and Smedler, G. *Appl. Catal. B: Environ.* **10**, 183 (1996).

Assanis, D., Filipi, Z., Gravante, A., Grohnke, D., Gui, X., Louca, L., Rideout, G., Stein, J., and Wang, Y. *SAE* 2000-01-0288 (2000).

Baba, N., Yokota, K., Matsunaga, S., Kojima, S., Ohsawa, K., Ito, T., and Domyo, H. *SAE* 2000-01-0214 (2000).

BASF "Urea solution 32.5% AdBlue", Technical Leaflet, BASF AG, Ludwigshafen, Germany (2003). Reference obtained from www.dieselnet.com/tech/cat_scr.html

Bissett, E. J. *Chem. Eng. Sci.* **39**, 1233 (1984).

Breen, J. P., and Burch, R. *Top. Catal.* **39**, 53 (2006).

Brogan, M. S., Brisley, R. J., Walker, A. P., Webster, D. E., Boegner, W., Fekete, N. P., Krämmer, M., Krutzsch, B., and Voigtländer, D. *SAE* 952490 (1995).

Burch, R., and Millington, P. J. *Catal. Today* **26**, 185 (1995).

Chandler, G. R., Cooper, B. J., Harris, J. P., Thoss, J. E., Uusimaki, A., Walker, A. P., and Warren, J. P. *SAE* 2000-01-0188 (2000).

Chatterjee, D., Burkhardt, T., Weibel, M., Tronconi, E., Nova, I., and Cristian, C. *SAE* 2006-01-0468 (2006).

Chorkendorff, I., and Niemantsverdriet, J. W., "Concepts of Modern Catalysis and Kinetics". Wiley-VCH, Weinheim (2003).

Clerc, J. C. *Appl. Catal. B: Environ.* **10**, 99 (1996).

Cooper, B. J., Jung, H. J., and Thoss, J. E. US Patent 4,902,487 (1990).

Dou, D., and Bailey, O. H. *SAE* 982594 (1998).

Dumesic, J. A., Topsøe, N.-Y., Topsøe, H., Chen, Y., and Slabiak, T. *J. Catal.* **163**, 409 (1996).

Evans, J. M., Ansell, G. P., Brown, C. M., Cox, J. P., Lafyatis, D. S., and Millington, P. J. *SAE* 1999-01-3472 (1999).

Fekete, N., Leyrer, J., Kemmler, R., and Krutzsch, B. *SAE* 970746 (1997).

Fluga, E. C. *SAE* 931179 (1993).

Forzatti, P. *Appl. Catal. A: Gen.* **222**, 221 (2001).

Fussey, P. M., Goodfellow, C. L., Oversby, K. K., Porter, B. C., and Wheals, J. C. *SAE* 2001-01-0938 (2001).

Gandhi, H. S., Graham, G. W., and McCabe, R. W. *J. Catal.* **216**, 433 (2003).

Gieshoff, J., Schafer-Sindlinger, A., Spurk, P. C., van den Tillaart, J. A. A., and Garr, G. *SAE* 2000-01-0189 (2000).

Haralampous, O. A., Koltsakis, G. C., Samaras, Z. C., Vogt, C.-D., Ohara, E., Watanabe, Y., and Mizutani, T. *SAE* 2004-01-0696 (2004).

Heck, R. M., and Farrauto, R. J. *Appl. Catal. A: Gen.* **221**, 443 (2001).

Huynh, C. T., Johnson, J. H., Yang, S. L., Bagley, S. T., and Warner, J. R. *SAE* 2003-01-0841 (2003).

Johnson, T. V. *SAE* 2004-01-0070 (2004).

Kandylas, I. P., and Koltsakis, G. C. *Ind. Eng. Chem. Res.* **41**, 2115 (2002).

Kleemann, M., Elsener, M., Koebel, M., and Wokaun, A. *Appl. Catal. B: Environ.* **27**, 231 (2000).

Koči, P., Marek, M., Kubíček, M., Maunula, T., and Härkönen, M. *Ind. Eng. Chem. Res.* **43**, 4503 (2004).

Koči, P., and Marek, M. *Chem. Eng. J.* **97**, 131 (2004).
Koebel, M., Elsener, M., and Madia, G. *MTZ—Motortechnische Zeitschrift* **62**, 35 (2001).
Koltsakis, G. C., and Stamatelos, A. M. *Prog. Energy Combust. Sci.* **23**, 1 (1997).
Konstandopoulos, A. G., and Johnson, J. H. *SAE* 890405 (1989).
Konstandopoulos, A. G., and Kostoglou, M. *Combust. Flame* **121**, 488 (2000).
Konstandopoulos, A. G., Kostoglou, M., Skaperdas, E., Papaioannou, E., Zarvalis, D., and Kladopoulou, E. *SAE* 2000-01-1016 (2000).
Konstandopoulos, A. G., Skaperdas, E., and Masoudi, M. *SAE* 2001-01-0909 (2001).
Konstandopoulos, A. G., Skaperdas, E., and Masoudi, M. *SAE* 2002-01-1015 (2002).
Kubo, S., Yamamoto, M., Kizaki, Y., Yamazaki, S., Tanaka, T., and Nakanishi, K. *SAE* 932706 (1993).
Lafyatis, D. S., Will, N. S., Martin, A. P., Rieck, J. S., and Cox, J. P. *SAE* 2000-01-0502 (2000).
Laing, P. M., Shane, M. D., Son, S., Adamczyk, A. A., and Li, P. *SAE* 1999-01-3476 (1999).
Lietti, L., and Forzatti, P. *J. Catal.* **147**, 241 (1994).
Lietti, L., Nova, I., Camurri, S., Tronconi, E., and Forzatti, P. *AIChE J.* **43**, 2559 (1997).
Marin, G. B., and Hoebink, J. H. B. J. *Cattech* **1**(2), 137 (1997).
Maurer, B., Jacob, E., and Weisweiler, W. *MTZ—Motortechnische Zeitschrift* **60**, 398 (1999).
Miyoshi, N., Matsumoto, S., Katoh, K., Tanaka, T., Harada, J., Takahashi, N., Yokota, K., Sugiura, M., and Kasahara, K. *SAE* 950809 (1995).
Nakanishi, Y., Dosaka, K., Iwama, K., Ishimaru, S., and Miki, M. US Patent 7 043 902 B2 (2006).
Nova, I., Castoldi, L., Lietti, L., Tronconi, E., Forzatti, P., Prinetto, F., and Ghiotti, G. *J. Catal.* **222**, 377 (2004).
Nova, I., Lietti, L., Tronconi, E., and Forzatti, P. *Catal. Today* **60**, 73 (2000).
Nova, I., Lietti, L., Tronconi, E., and Forzatti, P. *Chem. Eng. Sci.* **56**, 1229 (2001).
Oh, S. H., and Cavendish, J. C. *Ind. Eng. Chem. Prod. Res. Dev.* **21**, 29 (1982).
Rumpf, H., and Gupte, A. R. *Chemie-Ing. Tech.* **43**, 367 (1971).
Sahraeian, A., Shahbakhti, M., Aslani, A. R., Jazayeri, S. A., Azadi, S. A., and Shamekhi, A. H. *SAE* 2004-01-1620 (2004).
Schweich, D. Third International Congress on Catalysis and Automotive Control, *in* (A. Frennet, and J.-M. Bastin, Eds.), p. 55. Elsevier, New York (1995) (Stud. Surf. Sci. Catal. 96).
Stone, R., "Introduction to Internal Combustion Engines". Palgrave, New York, p. 261 (1999).
Takami, A., Takemoto, T., Iwakuni, H., Saito, F., and Koatsu, K. *SAE* 959746 (1995).
Twigg, M. V. *Appl. Catal. B: Environ.* **70**, 2 (2007).
Ullah, U., Waldram, S. P., Bennett, C. J., and Truex, T. *Chem. Eng. Sci.* **47**, 2413 (1992).
Voltz, S. E., Morgan, C. R., Liederman, D., and Jacob, S. M. *Ind. Eng. Chem. Prod. Res. Dev.* **12**, 294 (1973).
Wajsman, J., Champoussin, J. C., Dessalces, G., and Claus, G. *SAE* 960248 (1996).
Walker, A. P. *Catal. Today* **26**, 107 (1995).
Walker, A. P., Chandler, G. R., Cooper, B. J., Harris, J. P., Thoss, J. E., Warren, J. P., and Uusimaki, A. J. *SAE* 2000-01-0188 (2000).
Wanker, R., Granter, H., Bachler, G., Rabenstein, G., Ennemoser, A., Tatschl, R., and Bollig, M. *SAE* 2002-01-0066 (2002).
York, A. P. E., Ahmadinejad, M., Watling, T. C., Walker, A. P., Cox, J. P., Gast, J., Blakeman, P. G., and Allansson, R. *SAE* 2007-01-0043 (2007).
York, A. P. E., Cox, J. P., Watling, T. C., Walker, A. P., Bergeal, D., Allansson, R., and Lavenius, M. *SAE* 2005-01-0954 (2005).
York, A. P. E., Watling, T. C., Ahmadinejad, M., Bergeal, D., Phillips, P. R., and Swallow, D. FISITA World Congress, submitted for publication (2008).
York, A. P. E., Watling, T. C., Cox, J. P., Jones, I. Z., Walker, A. P., Blakeman, P. G., and Ilkenhans, T. *SAE* 2004-01-0155 (2004).
Zhang, Z., Yang, S. L., and Johnson, J. H. *SAE* 2002-01-1019 (2002).